

Article

Towards a Point-of-Care (POC) Diagnostic Platform for the Multiplex Electrochemiluminescent (ECL) Sensing of Mild Traumatic Brain Injury (mTBI) Biomarkers

Milica Jović , Denis Prim , Edis Saini and Marc Emil Pfeifer * 

Diagnostic Systems Research Group, Institute of Life Technologies, School of Engineering, University of Applied Sciences and Arts Western Switzerland (HES-SO Valais-Wallis), 1950 Sion, Switzerland; milica.jovic@hevs.ch (M.J.); denis.prim@hevs.ch (D.P.); edis.saini@lonza.com (E.S.)

* Correspondence: marc.pfeifer@hevs.ch; Tel.: +41-58-606-86-61

Abstract: Globally, 70 million people are annually affected by TBI. A significant proportion of all TBI cases are actually mild TBI (concussion, 70–85%), which is considerably more difficult to diagnose due to the absence of apparent symptoms. Current clinical practice of diagnosing mTBI largely resides on the patients' history, clinical aspects, and CT and MRI neuroimaging observations. The latter methods are costly, time-consuming, and not amenable for decentralized or accident site measurements. As an alternative (and/or complementary), mTBI diagnostics can be performed by detection of mTBI biomarkers from patients' blood. Herein, we proposed two strategies for the detection of three mTBI-relevant biomarkers (GFAP, h-FABP, and S100 β), in standard solutions and in human serum samples by using an electrochemiluminescence (ECL) immunoassay on (i) a commercial ECL platform in 96-well plate format, and (ii) a "POC-friendly" platform with disposable screen-printed carbon electrodes (SPCE) and a portable ECL reader. We further demonstrated a proof-of-concept for integrating three individually developed mTBI assays ("singleplex") into a three-plex ("multiplex") assay on a single SPCE using a spatially resolved ECL approach. The presented methodology demonstrates feasibility and a first step towards the development of a rapid POC multiplex diagnostic system for the detection of a mTBI biomarker panel on a single SPCE.

Keywords: biomarker panel; biosensor; electrochemiluminescence (ECL); electrochemiluminescence immunoassay (ECLIA); mild traumatic brain injury (mTBI); multiplex assay; point-of-care (POC) diagnostics; sandwich immunoassay; screen-printed electrode (SPE)



Citation: Jović, M.; Prim, D.; Saini, E.; Pfeifer, M.E. Towards a Point-of-Care (POC) Diagnostic Platform for the Multiplex Electrochemiluminescent (ECL) Sensing of Mild Traumatic Brain Injury (mTBI) Biomarkers. *Biosensors* **2022**, *12*, 172. <https://doi.org/10.3390/bios12030172>

Received: 14 February 2022

Accepted: 7 March 2022

Published: 11 March 2022

Publisher's Note: MDPI stays neutral with regard to jurisdictional claims in published maps and institutional affiliations.



Copyright: © 2022 by the authors. Licensee MDPI, Basel, Switzerland. This article is an open access article distributed under the terms and conditions of the Creative Commons Attribution (CC BY) license (<https://creativecommons.org/licenses/by/4.0/>).

1. Introduction

Traumatic brain injuries (TBI) are physical injuries that can lead to brain function alterations of temporary or permanent nature [1]. In the absence of routine diagnostic screening tests for TBI, the number of truly affected patients is difficult to assess and is probably significantly under-reported [2]. According to the CDC statistics, 1.5 million people suffer from TBI each year, while the most frequent causes of TBI are motor vehicle crashes, falls, and violence [3]. The Glasgow Coma Scale (GCS) developed in the seventies of the 20th century, is an assessment tool used to determine the consciousness level of the patient after a TBI, based on the ability to open eyes, be oriented, respond to questions, and obey motor commands [4]. Based on the extent of injury, TBIs can be classified as mild (GCS 13–15), moderate (GCS 9–12), and severe (GCS 3–8). A vast majority of TBI cases can be attributed to concussion, i.e., mild TBI [5]. Post-injury, there is often an absence of symptoms or primarily the presence of non-specific symptoms (e.g., headaches, fatigue, depression, visual and/or sleep disturbances, seizures, etc.) [6].

Diagnosis of mTBI can be rather challenging. The GCS scale is dependent on the assessment skills of the observer, and it can be inaccurate in distinguishing between mild and moderate TBIs [7]. Alternatives are neuroimaging tools, such as MRI and CT scans,

which can be quite costly, expose patients to harmful radiation, and are not available on-site (accident sites, sports fields, remote and underdeveloped areas, etc.). Also, approximately 90% of all mTBI cases will not have any evidence of structural abnormalities visible on a CT scan [8]. Therefore, there is a growing need to develop additional diagnostic screening tools for aiding diagnosis and enabling an accurate, inexpensive and fast triage of patients with mTBI [8–12].

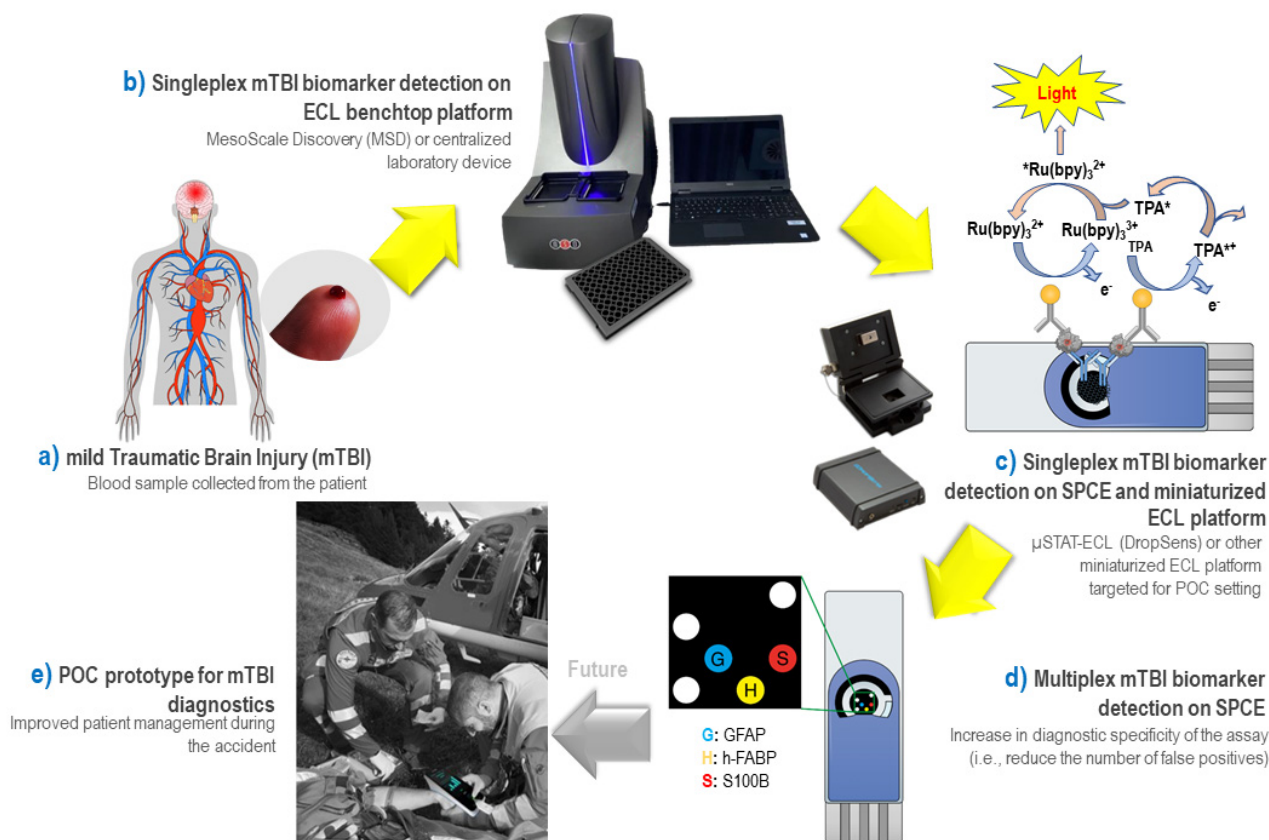
Biomarkers may have different intended uses, such as diagnostic, prognostic, predictive, pharmacodynamic, or efficacy response relevance. As for mTBI, the preferred ones are brain protein biomarkers that can pass the blood–brain barrier (BBB) into circulation. They can be found in human serum and/or plasma, and the analytical tools should be able to accurately detect them in the lower picogram range (pg mL^{-1}) [13]. The Scandinavian guideline proposes the use of the biomarker S100 calcium-binding protein β (S100 β) for mTBI patients who are admitted to the hospital within 6 h after the injury [14]. However, S100 β can be increased in multiple extra-cerebral tissues, for example, after extracranial injuries [15], peripheral lesions [16], and physical exercise [17].

Recently, several publications indicated other mTBI biomarkers that could be more suitable. For example, glial fibrillary acidic protein (GFAP) is a protein found in the cytoskeleton of glial cells [18] and has been used for the detection of acute intracranial injuries following a TBI [19]. The sensitivity of GFAP for the detection of intracranial lesions on CT scans has been reported to be 67% to 100%, with specificity between 0% and 100% [20]. GFAP could be useful for differentiating focal and diffuse brain injury; however, its ability to enter into the bloodstream depends on the BBB damage [21]. Furthermore, heart fatty-acid binding protein (h-FABP) is a cytosolic trafficking protein that can predict intracranial pathologies linked with brain injuries [22,23].

TBI biomarkers have the potential to significantly advance the way TBI is assessed and treated today, beyond the evaluation of the need for a head CT scan [24]. However, given the complexity of the TBI, it is unlikely that any single biomarker would be sufficiently sensitive and specific for use as a clinical diagnostic test. Posti et al. and Lagerstedt et al. reported on panels of protein biomarkers that perform better in discriminating CT positive from CT negative patients with mTBI than individual biomarkers [25,26]. As early as the beginning of 2018, a central laboratory test developed by Banyan Biomarkers was approved by the FDA [27]. The test is based on a chemiluminescent ELISA format for determining two TBI biomarkers, GFAP and ubiquitin carboxyl-terminal hydrolase isozyme L1 (UCH-L1), with a sensitivity of 97.5% for CT positive cases and a negative predictive value of 99.6% [27]. Practically the latter means that in more than 33% of the cases, the patients being suspected of brain injury can be ruled out prior to a CT scan [27]. Just recently, in January 2021, Abbott launched the POC diagnostic device i-STATTM AlinityTM that measures amperometrically UCH-L1 and GFAP [28], while the company NanoDxTM is in the progress of developing an ultrasensitive nanowire technology to resistively measure the S100 β and GFAP biomarkers [29].

Despite the recent developments in the mTBI diagnostic field, there is still a growing need to expand the biomarker panel with inflammatory and brain damage biomarkers to guarantee adequate diagnostic specificity and sensitivity and to allow decentralized mTBI diagnostics. To address these limitations, the conception of a minimally invasive multiplexed detection device would allow rapid and reliable detection of mTBI biomarkers at the POC level, which could revolutionize mTBI-patients management compared to conventional methods used. Many different electrochemical (EC) (bio)sensors approaches [30] and few ECL biosensor approaches have been proposed for detection of single, individual mTBI biomarkers (h-FABP [31,32]), but to the best of our knowledge, none using a mTBI biomarker panel. Electrochemiluminescence immunoassays (ECLIA) show great promise for the detection of low-level concentration compounds, with a wide linear range, high sensitivity, and low background noise [33]. In this work, we have developed a sandwich-type ECL assay for detecting and quantifying three mTBI-relevant biomarkers (GFAP, h-FABP and S100 β , Table 1), in standard solutions and in human serum samples

(HS), using a 96-well plate commercial “benchtop” platform from MesoScale Discovery (MSD) (Scheme 1b). These three individual “singleplex” assays were then translated into a miniaturized platform based on screen-printed carbon electrodes (SPCE) coupled with a portable ECL reader (μ STAT-ECL DropSens Metrohm, Scheme 1c). Furthermore, we showed a proof-of-concept for integration of three individually developed mTBI biomarker assays (“singleplex”) into a three-plex “multiplex” assay on a single SPCE using a spatially resolved ECL approach (Scheme 1d), demonstrating a first step towards the development of a POC diagnostic prototype instrument based on ECL detection of a mTBI biomarker panel (Scheme 1e).



Scheme 1. Schematic representation of a strategy proposed for the detection of blood proteins for mild traumatic brain injury (mTBI) diagnostics: (a) Illustration of the human body suffering from an mTBI injury and collection of blood sample potentially containing mTBI-relevant protein biomarkers. (b) Development of ECL-based sandwich immunoassay for each individual mTBI-relevant biomarker (“singleplex”) on a benchtop MesoScale Discovery (MSD) platform in 96-well plate format: (c) Translation of developed ECL detection strategy for each individual mTBI-relevant biomarker (“singleplex”) from benchtop MSD platform into a miniaturized “apropos Point-Of-Care (POC)” ECL platform based on screen-printed carbon electrodes (SPCE) and μ STAT-ECL reader from DropSens Metrohm. (d) Proof-of-concept for a multiplex ECL detection of three different mTBI-relevant biomarkers (i.e., GFAP, h-FABP and S100 β) on a single SPCE using a spatially resolved approach and a charge-couple device (CCD) camera as ECL detector. (e) Illustration of the envisioned POC diagnostic instrument in the context of medical emergencies allowing rapid treatment of patients following the accident. Steps (b–d) are achieved in the context of the present publication, while the step (e) represents the “ultimate” goal of the proposed methodology being the integration of the developed assays into the POC prototype for decentralized mTBI diagnostics (undeveloped areas, emergency rooms, battlefield, sports facilities, car accident sites, etc.).

Table 1. mTBI protein biomarkers used in this work and their clinically relevant concentration ranges.

Biomarker		Physiological Concentration ¹	
Abbreviation	Full Name	Normal	Mild TBI
GFAP	Glial fibrillary acidic protein	RG: 2–49 pg mL ⁻¹ [18] MD: 4 pg mL ⁻¹ [18]	≥33 pg mL ⁻¹ [18] CO: 22 pg mL ⁻¹ [27]
h-FABP	Heart-fatty acidic binding protein	<5.5 ng mL ⁻¹ [34] MN: 3.78 ng mL ⁻¹ [35]	CO: 2.62 ng mL ⁻¹ (HS/HP) [23]
S100β	S100β calcium-binding protein	MD: 50 pg mL ⁻¹ (HP) [36] <0.11 pg mL ⁻¹ [37]	≥100 pg mL ⁻¹ (HP) [38] >75 pg mL ⁻¹ [39] CO: 42 pg mL ⁻¹ (HS/HP) [23]

¹ Physiological concentration is indicated for human serum unless otherwise specified. Values reported in samples other than blood/serum/plasma (e.g., sweat, urine, muscle-on-tissue, etc.) are not considered. Abbreviations: CO—cutoff value; HP—human plasma; HS—human serum; MN—mean value; MD—median value; RG—range.

2. Materials and Methods

2.1. Materials

GFAP assay: Antigen GFAP human recombinant (ref. 8G45, HyTest Ltd., Turku, Finland); monoclonal mouse anti-human glial fibrillary acidic protein (ref. 4G25, HyTest Ltd., Turku, Finland) clone 83cc and clone 81cc were employed as capture and detection antibody, respectively.

h-FABP assay: Antigen FABP human (ref. 8F65, HyTest Ltd., Turku, Finland); monoclonal mouse anti-human fatty acid-binding protein (ref. 4F29, HyTest Ltd., Turku, Finland) clone 22 and clone 28cc were employed as capture and detection antibody, respectively.

S100β assay: Antigen S100BB homodimer and S100A1B heterodimer human (ref. 8S9h, HyTest Ltd., Turku, Finland); monoclonal mouse anti-human S100 proteins (ref. 4S37, HyTest Ltd., Turku, Finland) clone 8B10cc and clone 6G1cc were employed as capture and detection antibody, respectively.

Serum samples: Human serum from human male AB plasma, US origin, sterile filtered (ref. H4522, Sigma Aldrich, St. Louis, MO, USA) was diluted 2× with appropriate assay diluents and used for the recovery studies.

Other reagents: All chemicals were used as received without further purification. All aqueous solutions were prepared with MQ water. Gold SULFO-Tag NHS-Ester lyophilized (ref. RA19AO), read buffer T 4X (ref. R92TC), conjugation buffer (ref. R60AJ), conjugation storage buffer (ref. R60AC) and QuickPlex 96-well plate (ref. L55XA) were all purchased from Meso Scale Discovery (MSD). Other materials included: Zeba Spin desalting columns 40K MWCO 0.5 mL (87766, ThermoFisher, Waltham, MA, USA), Millex-GV Filter 0.22 μm (SLGV004SL, Sigma-Aldrich, MO, USA), syringe 1 mL BD Luer-Lok tip (309628, BD, New York, NJ, USA), casein sodium salt from bovine milk (C8654-500G, Sigma-Aldrich, MO, USA), bovine serum albumin fraction V (ref. 10735078001, Roche Diagnostics, Rotkreuz, Switzerland), PBS 10× pH 7.4 phosphate saline buffer (ref. 7011-044, Gibco, Billings, MT, USA), Tween-20 (ref. P1379-100 mL, Sigma-Aldrich, MO, USA), CaCl₂·2H₂O (ref. 223506, Fluka, Buchs, Switzerland). Technical grade ethanol was used for cleaning SPCE electrodes.

2.2. Apparatus

QuickPlex SQ120 (Meso Scale Discovery MSD): The MSD platform is based on ECL detection of a SULFO-Tag labelled detection antibody that emits light upon electrochemical stimulation. QuickPlex SQ120 was employed as an ECL plate reader for QuickPlex 96-well plates. The detection process is initiated on carbon electrodes located at the bottom of the wells, and only labels in the electrode proximity can be detected. The ECL mechanism of the co-reactant system ruthenium tris(bipyridine)-tripropylamine (read buffer) has been previously described [40].

Disposable screen-printed electrodes (SPEs, Metrohm DropSens): The SPEs incorporate a three-electrode setup, printed on ceramic substrates (size 33.0 mm × 10.0 mm). Both working (WE; disk-shaped 4-mm diameter) and counter-electrodes are fabricated from

carbon or carbon-based inks (for electrodes with modified WE), while pseudo-reference electrodes and electrical contact pads are fabricated from silver ink. An insulating layer is printed over the three-electrode system, leaving the electric contacts and a working area with an actual volume of 50 μ L. SPEs with different types of working electrodes were tested as the solid-state support throughout this work: screen-printed carbon electrodes (SPCE, ref. DRP-110), screen-printed carbon electrodes modified with gold nanoparticles (SPCE-GNP, ref. DRP-110-GNP), screen-printed carbon electrodes modified with carbon nanotubes and gold nanoparticles (SPCE-CNT-GNP, ref. DRP-110CNT-GNP) and screen-printed carbon electrodes modified with quantum dots (SPCE-QD, ref. DRP-110QD).

Homemade incubation cell for SPEs: Customized incubation cell for SPEs was fabricated from Teflon at the HES-SO Valais-Wallis mechanical workshop (Supplementary Figure S6). The cell was designed using the SolidWorks CAD package and was intended to fit 12 SPEs, leaving only the WE area to be exposed to the reagents during various incubation/mixing/washing steps of the immunoassay protocol. When the immunoassay protocol was finished, the SPEs were taken out of the incubation cell, washed with wash buffer solution, and transferred into μ STAT-ECL cell for the read-out.

μ STAT Bipotentiostat with ECL Cell (Metrohm DropSens): The device is composed of a potentiostat/galvanostat (± 4 V DC potential range, ± 40 mA maximum measurable current) (size 127.8 mm \times 124.1 mm \times 34.1 mm) combined with a detector that is integrated in the ECL cell (size 75.0 mm \times 88.4 mm \times 40.0 mm). The detector is a low-noise photosensor composed of a silicon photodiode with a spectral response range of 340–1100 nm, and a maximum sensitivity of 0.62 V/nW at 960 nm [41]. The device uses the DropView 8400 software for signal acquisition and can be employed as a portable, battery-operated ECL reader.

Multiplex electrode spotting with nano-spotter device: A S3 contactless nano-spotting device from Scienion AG (Berlin, Germany) equipped with a Piezo Dispense Capillary (PDC-70, coating type 3, p/n: P-2030 S-6051) was used to dispense drops of 300 pL on pre-defined positions of Metrohm DropSens electrodes.

Multiplex assay measurement imager: For ECL read-out from multiplex assay developed on SPE electrodes, a Vilber Fusion FX6 EDGE imager (Vilber Smart Imaging) was employed in combination with a μ STAT Bipotentiostat. The imager is equipped with an eVo6 scientific grade CCD camera (6.3 MPx, -30 $^{\circ}$ C cooling, $f/0.7$) to acquire signals generated from SPE. ImageJ software (v 1.53) was used for image processing.

2.3. Methods

Detection antibody conjugation with Ru(bpy)₃²⁺-NHS ester: Detection antibody labeling with Gold SULFO-Tag NHS-Ester was performed following the protocol provided by MesoScale Discovery (MSD GOLD SULFO-TAG Conjugation Quick Guide). Challenge ratio of 50:1 was used for all detection antibodies, while the labeling incorporation ratio was calculated based on the OD₄₅₅ measured for each labelled antibody using the NanoDrop OnceC Microvolume UV-VIS Spectrophotometer (Thermo-Fisher Scientific, Waltham, MA, USA). The calculated label ratio was 19:1, 14:1 and 21:1 for GFAP, h-FABP and S100 β detection antibodies, respectively.

Singleplex assay on MSD platform: 30 μ L of capture antibody (at desired concentration, diluted in the appropriate coating diluent) was added in the well of QuickPlex 96-well plate. After the incubation step (1.5 h, room temperature RT, 700 rpm) the plate was washed using a dedicated wash buffer (3 \times 300 μ L), and 100 μ L of blocking agent was added (45 min, RT, 700 rpm). After the second washing step, 30 μ L of antigen or blank was added in the well and incubated (1 h, RT, 700 rpm). After the third washing step, 30 μ L of detection antibody was added at desired concentration (diluted in corresponding diluent) and incubated (1 h, RT, 700 rpm). After the final washing step, 150 μ L of MSD read buffer 2 \times was added in each well and ECL signal was recorded using MSD QuickPlex SQ120 plate reader.

Singleplex assay on SPCEs: SPCEs were firstly washed using the mixture of ethanol/water (2:1) for 20 min, then rinsed with DI water, dried with nitrogen, and placed

inside the “homemade” incubation cell. The immunoassay protocol was identical as described in the paragraph above for MSD platform, with the difference that all incubation steps were performed at 500 rpm. After the last incubation/washing step, the SPCEs were taken out from the incubation cell and placed inside the ECL cell of μ STAT-ECL instrument with 50 μ L of MSD read buffer 2 \times to perform the read-out.

Multiplex assay on SPCEs: Electrodes were cleaned using the same protocol as described for the *singleplex* assay. The multiplex assay was performed using the assay conditions established for S100 β biomarker (Table 2). The capture antibodies (50 μ g mL⁻¹) were deposited on the working electrode using the automated nano-spotter device (S3, Scienion, Berlin, Germany) by collocated spotting of 30 drops of 300 pL (\pm 10 pL), to form spots of 250 μ m (\pm 50 μ m) diameter. The source plate temperature was set at RT and the relative humidity in the spotting area at 60%. After deposition, SPCEs were let in the spotting area during 30 min before blocking with 2% BSA for 1 h at RT and washing with wash buffer. Incubation with antigen and detection antibodies was carried out in homemade incubation cells for SPEs. The read-out was performed with 150 μ L of MSD read buffer 2 \times using Vilber Fusion FX6 EDGE imager (Vilber Smart Imaging) combined with μ STAT Bipotentiostat.

3. Results

3.1. Development of ECL “Singleplex” Assays for mTBI Biomarkers on MSD Platform

MSD QuickPlex SQ120 is a versatile and robust platform that can be very useful tool for the detection of different types of analytes in 96-well plate format, and it was employed for development of ECL sandwich immunoassays for each of the individual mTBI biomarkers (GFAP, h-FABP and S100 β) (Scheme 1b).

A design of experiment (DoE) approach was used to determine the optimal settings and conditions for the major controllable factors in the assay. The following conditions were jointly assessed for development/optimization of each individual mTBI biomarker assay:

- Coating diluent (PBS 1 \times pH 7.4 or TRIS 50 mM pH 8.6, with addition of 0.1–5 mM CaCl₂ for S100 β assay)
- Blocking agent (0.1–2% of BSA or 0.1–2% casein in PBS 1 \times pH 7.4 or TRIS 50 mM pH 8.6, with/without addition of 0.1% Tween-20);
- Wash buffer (PBS 1 \times pH 7.4 or TRIS 50 mM pH 8.6, with 0.05–0.4% Tween-20);
- Detection antibody diluent (PBS 1 \times pH 7.4 or TRIS 50 mM pH 8.6, with/without addition of 0.1–1% of blocking agent and/or 0.06% Tween-20);
- Capture antibody (cAb) and detection antibody concentration (dAb) (cAb concentration range: 1–25 μ g mL⁻¹; dAb concentration range: 0.5–10 μ g mL⁻¹).

Table 2 summarizes the pre-optimized assay conditions obtained for each individual mTBI biomarker. In overall, the optimized assay conditions for GFAP and h-FABP assay were very similar. The optimal blocking agent was 1% BSA and all diluents were based on PBS 1 \times . In the case of the S100 β assay, all diluents were based on 50 mM TRIS buffer (pH 8.6) with the addition of CaCl₂, due to the fact that the S100 protein is a dimeric member of the EF-hand calcium-binding protein superfamily, and its calcium-binding properties influencing the antibody recognition [42,43]. Several studies indicated that such interaction happens through a calcium-induced conformational change, which leads to the exposure of a hydrophobic protein region [42].

Table 2. Preliminary conditions evaluated on MSD platform for each individual mTBI biomarker ECL sandwich immunoassay (*singleplex*).

mTBI Biomarker	cAb Diluent	Blocking Agent	Assay Diluent	Wash Buffer	dAb Diluent	cAb Conc. ($\mu\text{g mL}^{-1}$)	dAb Conc. ($\mu\text{g mL}^{-1}$)	LOD (pg mL^{-1})	Range (pg mL^{-1})
GFAP	PBS 1×	1% BSA; 0.06% Tween-20; PBS 1×	MQ water	0.06% Tween-20; PBS 1×	1% BSA; PBS 1×	25.00	2.50	6.94 [6.9–10.0; CI:95%]	0–10,000
h-FABP	PBS 1×	1% BSA; 0.06% Tween-20; PBS 1×	PBS 1×	0.06% Tween-20; PBS 1×	1% BSA; PBS 1×	5.00	0.50	1.35 [0–4.4; CI:95%]	0–10,000
S100 β	5 mM CaCl ₂ ; 50 mM TRIS	2% BSA; 1 mM CaCl ₂ ; PBS 1×	0.1% BSA; 1 mM CaCl ₂ ; 50 mM TRIS	0.06% Tween-20; PBS 1×	0.1% BSA; 1 mM CaCl ₂ ; 50 mM TRIS	10.00	5.00	15.73 [11.0–20.5; CI:95%]	0–10,000

In some publications, the authors reported that the addition of Ca²⁺ in the antibody diluents had as a consequence, an improvement of the recognition activity [44,45], while others reported that calcium-chelators improved the antigen recognition (immunoassays with Sangtec antibodies) [46]. In the present study, we noticed that the addition of Ca²⁺ in the coating, assay and detection antibody diluent had a positive impact on the assay performance. This is also supported by the fact that the antibody provider recommends add it the ion of Ca²⁺ in the antibody diluents. Concentrations of capture and detection antibody were optimized for each biomarker using the mean matrix heatmap format. The results are presented in Figure 1 (left figures) as a heat map showing the signal intensities (GFAP assay) and S/B ratios (h-FABP and S100 β assay) from low (red) to high (green). The capture and detection antibody concentrations were determined based on the maximum S/B results, apart from GFAP assay, where the antibody concentrations were chosen based on the highest signal intensities.

To evaluate the analytical performance of each *singleplex* biomarker assay, buffer solutions containing each individual biomarker concentration ranging from 10 pg mL⁻¹ to 10 ng mL⁻¹ were analyzed. Based on the obtained results, a calibration curve (Figure 1, right figures) was established for each biomarker using the pre-optimized conditions from Table 2. Data were analyzed by assuming that the ECL intensity was proportional to the biomarker concentration through a four-parameter dose-response regression function (4PL) model with 1/Y² weighting (OriginPro software). To fit the data, the following equation was used (Equation (1)):

$$y = \frac{A_1 - A_2}{1 + \left(\frac{x}{x_0}\right)^p} + A_2 \quad (1)$$

where x denotes the concentration of the biomarker, and A_1 , A_2 , x_0 , and p are the four parameters. The A_1 and A_2 parameters correspond to the upper and lower asymptotes for the function, respectively, while the p (Hill slope) and x_0 parameters correspond to the slope.

As Figure 1 indicates, the developed *singleplex* assays had good dynamic ranges, background levels, and sensitivities. The LOD values were calculated by interpolating the curve using the average value of the blank plus three times the standard deviation of the blank. Obtained LOD values of 6.94 pg mL⁻¹ ($R^2 = 0.9999$), 1.35 pg mL⁻¹ ($R^2 = 0.9999$) and 15.73 pg mL⁻¹ ($R^2 = 0.9999$) were achieved for GFAP, h-FABP and S100 β biomarker, respectively.

Once the suitability for mTBI biomarker panel detection has been established on the MSD platform, the assays were translated to SPE-based ECL test set-up platform.

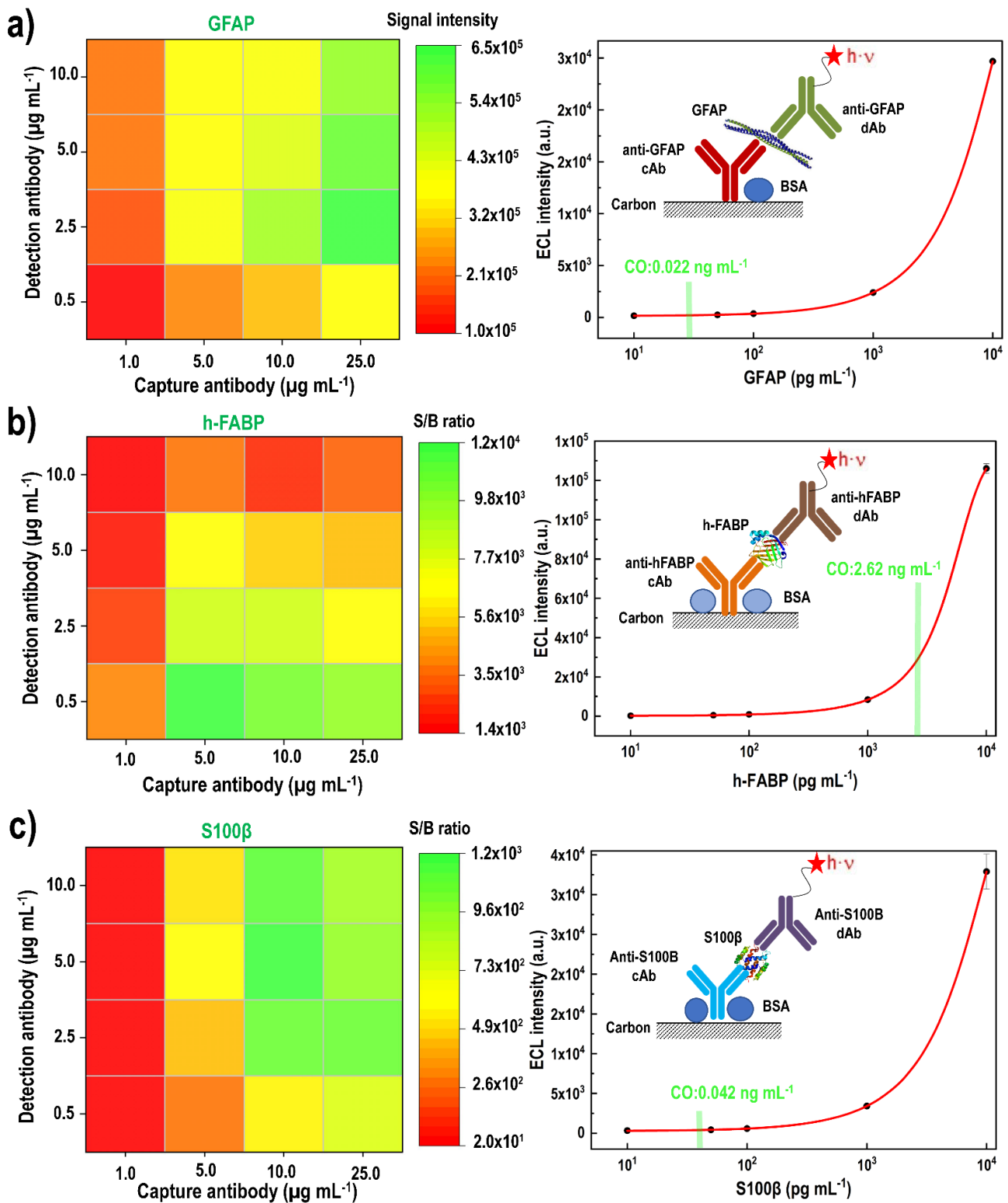


Figure 1. ECL sandwich immunoassays for mTBI-relevant biomarkers on the MSD platform in a 96-well plate format: (a) GFAP, (b) h-FABP, and (c) S100β. Left figures—Optimization of antibody concentrations in the sandwich assay: checkerboard optimization assay for the antibody pairs with the *x*-axis representing the capture antibody concentrations and the *y*-axis the detection antibody concentrations. The results are visualized as a heat map plot with reported signal intensities or S/B ratios (100 ng mL⁻¹/blank). Right figures—ECL calibration curves established using the conditions listed in Table 2. The error bars represent the standard deviation from three replicates; bars are smaller than the data symbol employed. CO—cutoff value for the biomarker.

3.2. Development of ECL “Singleplex” Assays for mTBI Biomarkers on SPE

3.2.1. Choice of Electrode Material

The use of SPE in the context of highly sensitive ECL analytical and electrochemical diagnostic applications requires several different electrode characteristics such as: (a) fast electron transfer; (b) reproducible electrode surfaces that can improve the assay accuracy and precision; (c) large electroactive electrode areas to boost signal intensities; (d) broad potential window; and (e) a hydrophobic electrode surface to facilitate TPA oxidation on the electrode surface [47–49]. Hence, four commercially available SPEs were investigated for an application in ECL detection of mTBI biomarkers: SPCEs (DRP-110), SPCEs modified with gold nanoparticles SPCE-GNP (DRP-110-GNP), SPCEs modified with carbon nanotubes and gold nanoparticles SPCE-CNT-GNP (DRP-110CNT-GNP), and SPCEs modified with quantum dots SPCE-QD (DRP-110QD).

Firstly, the electrochemical properties of each electrode were tested using a standard redox couple (ferri/ferrocyanide) (Table 3). All electrodes showed quasi-reversible electrochemical behavior with the peak-to-peak separation (ΔE) higher than anticipated for the one-electron transfer process (>59 mV). The values were consistent with the ones reported by Banks et al. [50] and Fanjul-Bolado et al. [51] stating that it arises from a combination of the electrode properties (electrode material, composition of the paste used for the fabrication, the curing temperature, the hydrophilic characteristics of the electrode surface) [49]. The electrode electro-active area (A) was calculated using the Randles–Sevcik equation (Equation (2)) by studying the scan rates of 5 mM $K_4[Fe(CN)_6]/K_3[Fe(CN)_6]$ in 0.1 M PBS) [52]:

$$i_p = (2.69 \times 10^5) \cdot n^{3/2} \cdot A \cdot C \cdot D^{1/2} \cdot \nu^{1/2} \quad (2)$$

i_p is the peak current (A), n is the number of electrons involved in the redox reaction, A is the active electrode area (cm^2), C is the concentration of redox molecule (mol/cm^3), D is the diffusion coefficient (cm^2/s), and ν is the scan rate (V/s).

Table 3. Electrochemical properties of tested commercially available SPEs.

SPE	Product Number	A (cm^2) *	ΔE (mV)	I_a/I_c
SPCE	DRP-110	0.1540	150	1.04
SPCE-GNP	DRP-110-GNP	0.1580	180	1.00
SPCE-CNT-GNP	DRP-110CNT-GNP	0.1470	285	1.03
SPCE-QD	DRP-110QD	0.0270	270	1.00

* Calculated using Equation (2), (average $n = 3$).

The representative cyclic voltammograms showing the scan rate studies with ferri/ferrocyanide couple on different SPEs are shown in Figure S2a. SPCE and SPCE-GNP electrodes showed the highest active electrode area (A) and the highest conductivity (the lowest peak-to-peak separation, ΔE). Electrochemical properties of each electrode material were also tested with $[Ru(bpy)_3]^{2+}$ in PBS 1×. All CVs showed a reversible oxidation peak at ~ 0.5 V vs. Ag and a corresponding reduction peak at ~ 0.3 V vs. Ag pseudo-reference electrode (illustrated in Figure S2b).

Furthermore, to be able to compare the SPEs in terms of relative ECL intensities, a commercial solution containing $[Ru(bpy)_3]^{2+}$ and TPA (MSD Free Tag 15,000) was used to generate ECL signal upon applying the potential on SPEs (Figure 2). In that context, SPCE electrodes showed the highest ECL intensities, followed in decreasing order by SPCE-GNP > SPCE-CNT-GNP > SPCE-QD.

Since SPCEs showed the best electrochemical performance and exhibited the highest ECL intensity (Figure 2), they were selected as solid-state support for development of mTBI assays. SEM images of SPCE electrodes are shown in Figure S3.

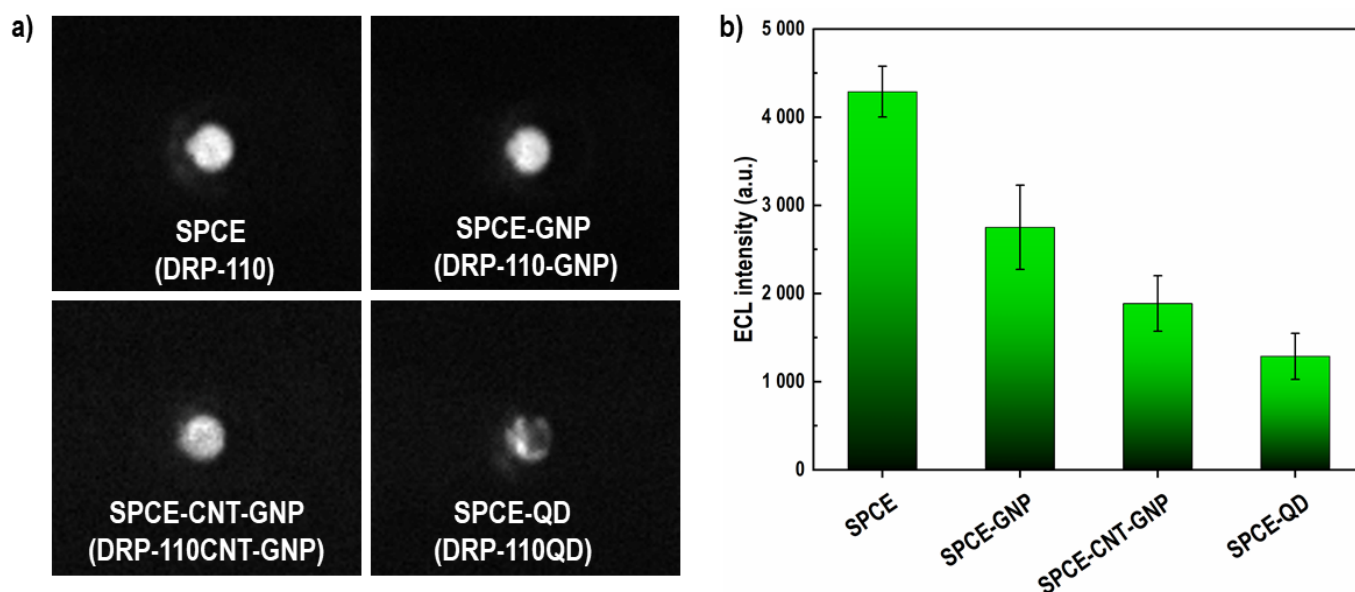
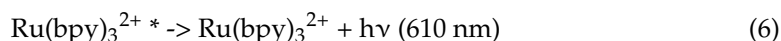
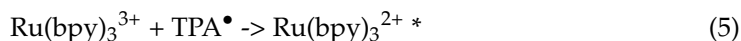
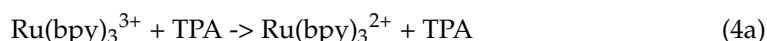
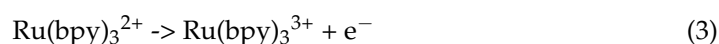


Figure 2. (a) Representation of ECL images obtained from four different commercial screen-printed electrodes (SPEs) using Vilber Fusion FX6 EDGE (Vilber Smart Imaging) (MSD Free Tag solution 15,000 a.u., 100 μ L, LSV 200 mV/s, 0.1–1.8 V); (b) ECL intensity ($n = 3$) calculated by integration of light spot using ImageJ software, errors bars correspond to STDEV. Electrodes tested: SPCE (DRP-110), SPCE-GNP (DRP-110-GNP), SPCE-CNT-GNP (DRP-110CNT-GNP), and SPCE-QD (DRP-110QD).

3.2.2. Optimization of SPCE-Based ECL Sensor

The ECL signal of the co-reactant couple $\text{Ru}(\text{bpy})_3^{2+}$ –TPA is produced via the reaction between the deprotonated TPA radical (TPA^\bullet) and electrogenerated $\text{Ru}(\text{bpy})_3^{3+}$, forming a $[\text{Ru}(\text{bpy})_3^{2+}]^*$ radical that generates light emission when returning to the ground state (Equations (3)–(6)). TPA can be created via catalytic oxidation by electrogenerated $\text{Ru}(\text{bpy})_3^{3+}$ (Equation (4a)) and direct electrode oxidation (Equation (4b)) [53]. Figure 3a shows an exemplary linear sweep voltammetric curve of SPCE (black line) and generated ECL curve (red line) obtained for h-FABP assay indicating a strong ECL peak at ~ 1.3 V vs. Ag electrode.



Furthermore, two options were evaluated for the ECL signal trigger from SPCE: for (i) linear sweep voltammetry (LSV) (Figure 3a), versus (ii) constant potential chronoamperometry (CPA) (Figure 3b). For LSV, the scan rate of 200 mV/s for LSV has been selected considering that higher scan rates led to broadening and shift of ECL peak towards positive potentials, which consequently led to water oxidation, causing the formation of bubbles on the electrode surface that had a negative impact on detected ECL signals. For CPA three different potentials were tested: 1.4, 1.5, 1.55, and 1.6 V.

ECL signals generated by LSV were ~ 800 a.u. (Figure 3a), while for CPA it was found that the ECL signal intensity increased as the applied potentials became more positive, showing the maximum value of ~ 2250 a.u. at 1.55 V vs. Ag electrode (Figure 3b—insert plot). Based on these results it was decided to use CPA for the further experiments and development of mTBI biomarker assay on SPCE electrodes.

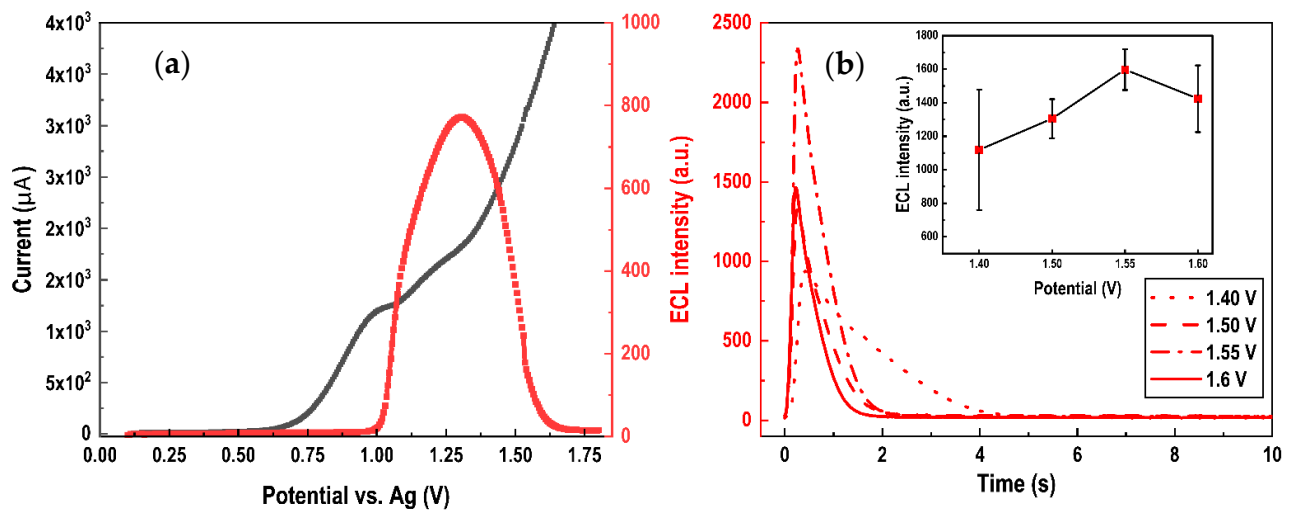


Figure 3. (a) Linear sweep voltammogram of SPCE for h-FABP biomarker assay (scan rate 200 mV/s) (black curve) and generated ECL signal (red curve). (b) ECL intensity curves from h-FABP biomarker assay on SPCE generated by chronoamperometry at different potentials: 1.4; 1.5; 1.55 and 1.6 V. Acquisition time 10 s. h-FABP assay conditions in Table 4 below (antigen concentration 100 ng mL⁻¹).

Table 4. Preliminary conditions evaluated on SPCE using μ STAT-ECL platform for each individual mTBI biomarker ECL sandwich immunoassay (*singleplex*).

mTBI Biomarker	cAb Diluent	Blocking Agent	Assay Diluent	Wash Buffer	dAb Diluent	cAb Concentration ($\mu\text{g mL}^{-1}$)	dAb Concentration ($\mu\text{g mL}^{-1}$)	LOD	Dynamic Range
GFAP	PBS 1 \times	1% BSA; 0.06% Tween-20; PBS 1 \times	MQ water	0.06% Tween-20; PBS 1 \times	1% BSA; PBS 1 \times	25.00	2.50	0.59 ng mL ⁻¹	0–50 ng mL ⁻¹
h-FABP	PBS 1 \times	1% BSA; 0.06% Tween-20; PBS 1 \times	PBS 1 \times	0.06% Tween-20; PBS 1 \times	1% BSA; PBS 1 \times	5.00	0.50	0.44 ng mL ⁻¹	0–50 ng mL ⁻¹
S100 β	5 mM CaCl ₂ ; 50 mM TRIS	2% BSA; 1 mM CaCl ₂ ; PBS 1 \times	1 mM CaCl ₂ ; 50 mM TRIS	0.06% Tween-20; PBS 1 \times	0.1% BSA; 1 mM CaCl ₂ ; 50 mM TRIS	25.00	12.50	1.34 ng mL ⁻¹	0–50 ng mL ⁻¹

3.2.3. Optimization of the Assay Conditions

The pre-optimized assay conditions obtained for each mTBI biomarker on the MSD platform (Table 2) were translated to the SPCE and μ STAT-ECL platform, with the only difference that the concentrations of capture and detection antibodies were re-optimized using the checkerboard assay due to the differences in the WE area and morphology between MSD and SPCE electrodes (cAb-dAb ratio was kept constant, Table 4). The results are presented in Figure 4 (left figures) as a heat map showing the S/B ratios from low (red) to high (green). The optimal capture and detection antibody concentrations were determined based on the maximum S/B results and summarized in Table 4.

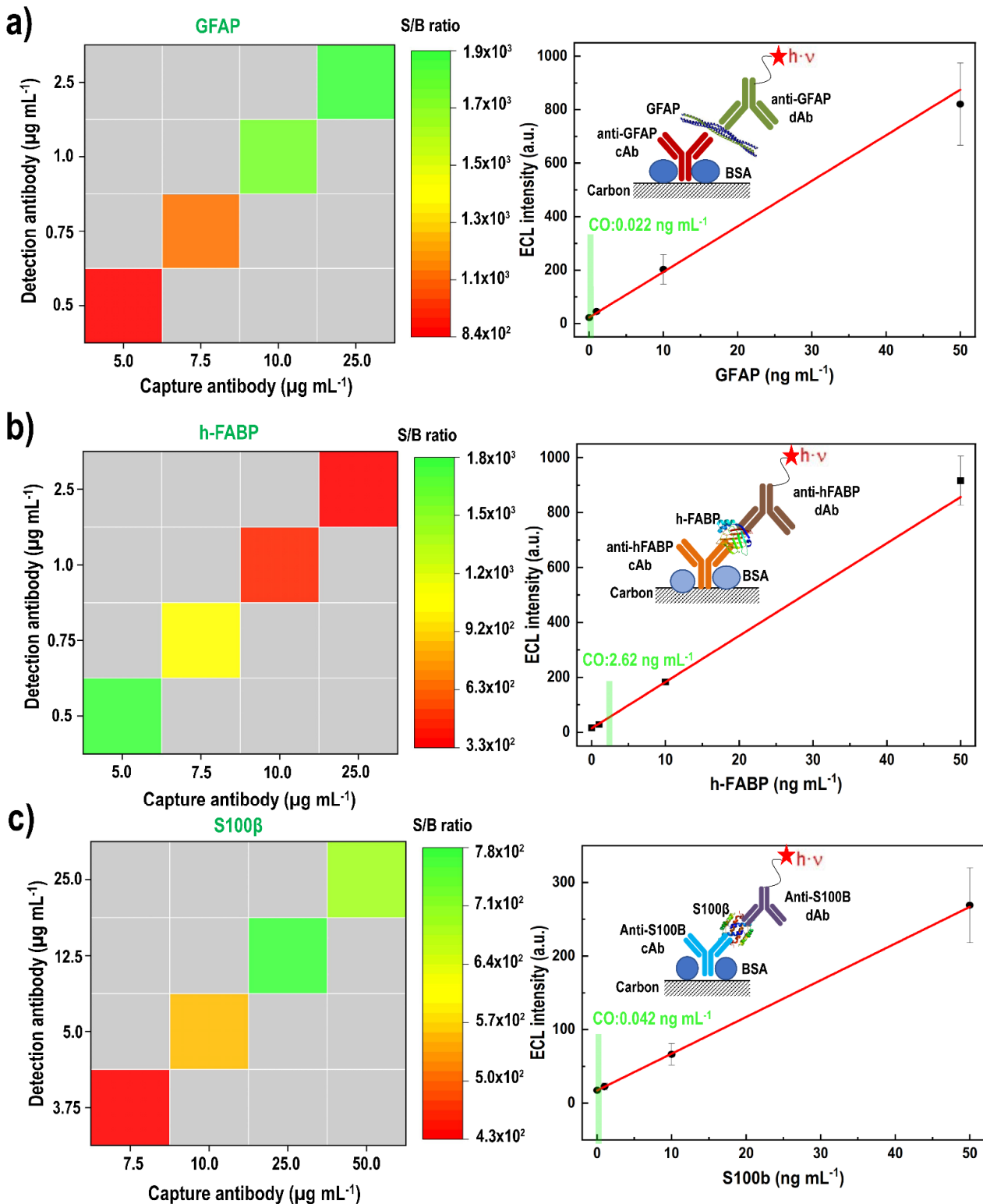


Figure 4. ECL immunoassays for mTBI-relevant biomarkers on SPCE μ STAT-ECL platform: (a) GFAP, (b) h-FABP, and, (c) S100 β . Left figures—Optimization of antibody concentrations in the assay: checkerboard optimization assay for the antibody pairs with the x -axis containing the capture antibody concentrations and the y -axis the detection antibody concentrations (capture/detection antibody ratio 10/1). The results are presented as a heat map plot with reported S/B ratios (100 ng mL $^{-1}$ /blank). Right figures—ECL calibration curve established using the conditions listed in Table 4. The error bars represent the standard deviation from three replicates ($n = 3$); bars are smaller than the data symbol employed.

Analytical performance of the developed *singleplex* mTBI assays on the SPCEs was evaluated using the buffer samples containing each individual biomarker concentration ranging from 1 ng mL⁻¹ to 50 ng mL⁻¹ using pre-optimized conditions from Table 4. Based on the measured values, a calibration curve (Figure 4) was modeled by the linear regression equations for each mTBI biomarker (n = 3) (Figure S4). The LOD values were calculated using the average value of the blank and adding to it three times the standard deviation of the blank. LOD values of 0.59 ng mL⁻¹ (R² = 0.9777), 0.44 ng mL⁻¹ (R² = 0.9931) and 1.34 ng mL⁻¹ (R² = 0.9984) were achieved for GFAP, h-FABP and S100β, respectively.

3.3. Standard Recovery Test

The applicability and reliability of developed mTBI biomarker assays, on both ECL instrument platforms, were evaluated in a complex physiological matrix by standard addition method. Different concentrations of biomarkers were added in human serum diluted 2× with respective assay diluents (defined as “spiked” concentration). Based on the obtained ECL signal intensity, the corresponding biomarker concentrations (defined as “detected” concentration) were calculated according to the regression equation performed using the same matrix (4PL dose-response curve). The recoveries were calculated by the ratio between the “detected” and “spiked”, and the obtained results are summarized in Table 5 (Figure S5). It could be seen that the recoveries ranged from 79% to 128%, which seems acceptable at this development stage. These results suggest that with further development and optimization, these assays have a potential for future mTBI clinical diagnostic applications.

Table 5. Results of the recovery test for mTBI biomarkers in human serum (HS, n = 2) samples diluted 2× with respective assay diluent (details of the assay conditions are listed in Table 2).

Sample	Added Biomarker	Spiked Concentration (ng mL ⁻¹)	Detected Concentration by MSD (ng mL ⁻¹)	Recovery (%)	Detected Concentration by μSTAT-ECL (ng mL ⁻¹)	Recovery (%)
Human serum	h-FABP	0	0	/	0	/
		2.50	2.30	92%	1.99	79%
		5.00	4.37	87%	5.33	106%
	GFAP	0	0	/	0	/
		2.50	2.23	89%	2.62	105%
		5.00	5.30	106%	4.34	87%
	S100β	0	0	/	0	/
		2.50	2.43	96%	2.11	84%
		5.00	6.41	128%	5.92	118%

3.4. Multiplex ECL Assay for mTBI Biomarker Panel on SPCE

Once the *singleplex* assays have been developed on SPCE (GFAP, h-FABP, S100β) they were integrated into a multiplexed assay with the goal to enable high-throughput simultaneous detection of multiple mTBI biomarkers on a single electrode.

SPCEs were spotted with capture antibodies of each biomarker (14 nL/spot, diameter ~500 μm) and with BSA protein labelled with SULFOTAG (alignment spots on the electrodes) (Figure 5), and the assay protocol was performed as described in Section 3.3 (S100β diluents were used as common diluents for all three biomarkers). Different electrode patterns were prepared, as described in Figure 5a–e. Obtained results indicated no cross-reactivity between the antibodies, providing a proof-of-concept that the present methodology based on spatially resolved approach can serve as a foundation for simultaneous, single electrode, detection of a mTBI biomarker panel, and other multi-biomarker panels (e.g., cardiac).

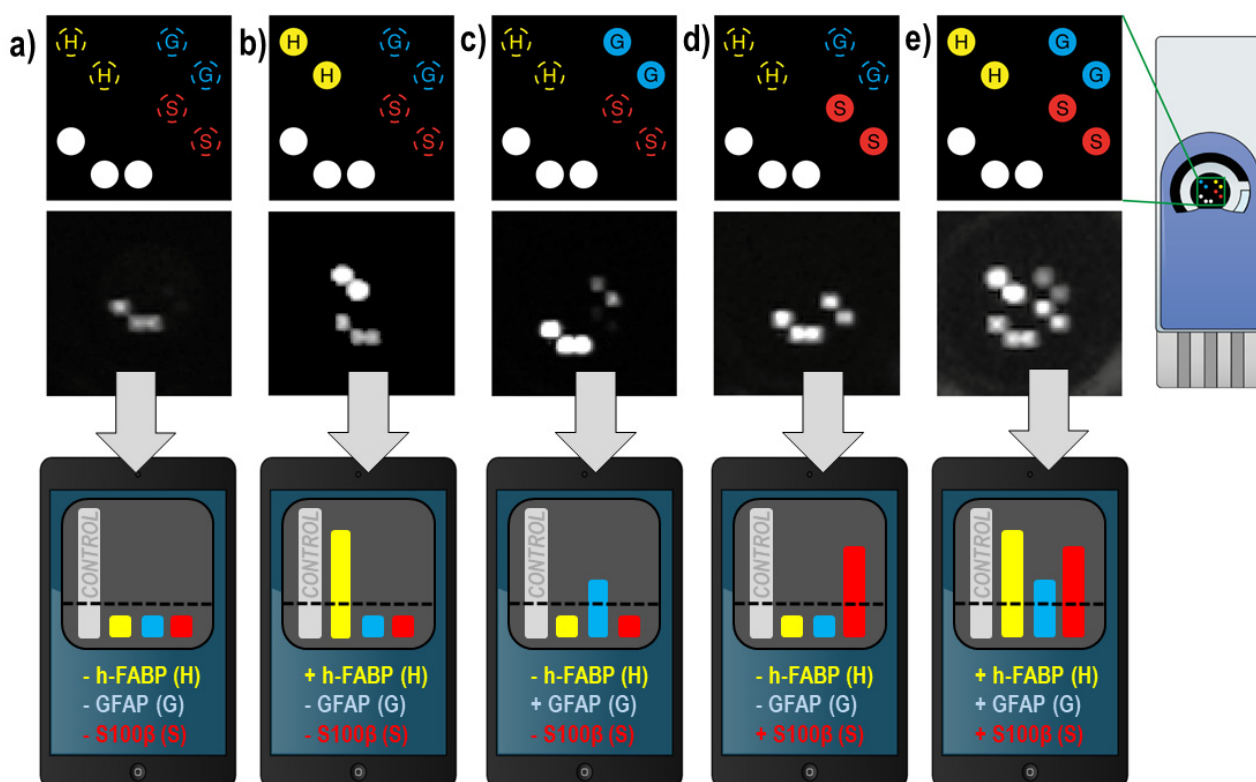


Figure 5. Multiplex ECL detection of mTBI biomarker panel established on a single SPCE. Top panel figures indicate the electrode patterns that contain alignment spots (“control”) made with BSA protein labelled with SULFO-TAG (white spots); spots for GFAP biomarker (blue spots with letter “G” indicate the position of GFAP capture antibodies); spots for h-FABP biomarker (yellow spots with letter “H” indicate the position of h-FABP capture antibodies); and spots for S100 β biomarker (red spots with letter “S” indicate the position of S100 β capture antibodies). Dashed letter spots indicate that no antigen was added (blank), while full-colored letter spots indicate that respective antigen was added in the assay. Middle panel figures respectively show real ECL images obtained from the electrode pattern indicated on top panel images, and bottom panel figures show the concept of the signal read-out displayed for the future envisioned mTBI POC diagnostic device: (a) biomarkers not detected in the sample (only three “control” spots are visible); (b) h-FABP biomarker detected; (c) GFAP biomarker detected; (d) S100 β biomarker detected; (e) all three biomarkers detected.

4. Discussion

The purpose of this study was to evaluate the feasibility of developing a multiplex ECL assay for mTBI biomarkers targeted for a POC diagnostic format and to identify the most important steps that need to be conquered on the way.

Firstly, ECL assays for three mTBI biomarkers (GFAP, h-FABP, S100 β) have been developed on a reference benchtop ECL platform from MesoScale Discovery (96-well plate format). The analytical performances of these *singleplex* assays were impressive, reaching LODs of 6.94 pg mL⁻¹, 1.35 pg mL⁻¹ and 15.73 pg mL⁻¹ for GFAP, h-FABP and S100 β biomarker, respectively. The obtained LODs were close or below 1/10 of the cut-off values reported for these three biomarkers (22 pg mL⁻¹, 2.62 ng mL⁻¹ and 42 pg mL⁻¹, Table 1), indicating that the developed assays have analytical sensitivities to distinguish a “mTBI condition” from “normal”, physiological concentration of the specific biomarker.

When comparing the obtained results with other published ECL-based methodologies, it is worth mentioning the work of Button et al., who reported a sandwich immunoassay for detection of GFAP biomarker on MSD platform in mouse plasma samples, with a LOD of 9 pg mL⁻¹ [54]. Roche Diagnostics provides ECL-based immunoassay for the *in vitro* diagnostic quantitative determination of S100 β in human serum based on Elecsys[®]

technology on Cobas instruments, with reported LOD of 15 pg mL^{-1} [55]. Gan et al. reported an ECL immunosensor for detection of h-FABP biomarker using luminophore coupled with 2D metal-organic framework (LOD of 44.5 fg mL^{-1}) [31]. Regarding the methodologies reported for detection of mTBI biomarkers suitable for POC settings, it is worth mentioning the lateral flow immunoassay (LFIA) approaches reported by Natarajan and Joseph [56] for rapid detection of GFAP biomarker (time-resolved fluorescence read-out, 25 min detection time, LOD 10 pg mL^{-1}), the approach of Savin et al. [57] for detection of h-FABP biomarker (CdTe quantum dots labelled detection antibodies, LOD 221 pg mL^{-1}), and the approach developed by Gao et al. [58] for detection of S100 β (surface-enhanced Raman spectroscopy read-out, LOD 5 pg mL^{-1}). A detailed list of other methodologies published so far in the context of detection of GFAP, h-FABP and S100 β biomarkers is given in Table S1.

Even though the MSD platform allows facile assay development and optimization, the instrument is not suitable for POC diagnostics and particularly not for on-site accident applications due to the size, weight, and cost limitations. Thus, the ECL assays for mTBI biomarkers have been translated to screen-printed electrodes (SPEs) coupled with a (trans-)portable μ STAT-ECL reader from Metrohm DropSens (see Section 2.1). SPEs are an attractive choice for realizing POC-oriented devices due to their low cost, mass fabrication, small sample volume requirements, and ability to be easily integrated and miniaturized [59]. SPEs can be easily combined with ECL detection to achieve a cost-effective, simplified POC diagnostic device.

One of the most important electrode aspects in the context of ECL detection is the electrode material. Our results have shown that non-modified SPCE exhibit better performances in the ECL assays than all other tested electrodes from Metrohm DropSens (SPCE-GNP, SPCE-CNT-GNP, or SPCE-QD). A similar observation was also reported (excluding SPCE-QD) in the work of Kerr et al. [49]. Unmodified carbon is often chosen for WE since it is a cheap, widely commercially available material that exhibits rapid and efficient oxidation of TPA, is relatively hydrophobic, allowing high concentrations of TPA on the electrode surface, and has low rates of surface oxide formation compared to noble metal electrodes [49,52]. Furthermore, two different electrochemical techniques were employed for ECL signal trigger, linear sweep voltammetry (LSV) and constant potential chronoamperometry (CPA). The obtained results showed that CPA at 1.55 V increased $\sim 3\times$ the ECL signal intensities in the assay compared to the LSV (Figure 3b).

Even though in the literature there are plenty of ECL biosensors based on screen-printed electrodes [60], to the best of our knowledge, this is the first study showing the development of ECL assays on SPCE combined with the miniaturized μ STAT-ECL reader from Metrohm DropSens [41]. The LOD values of 0.59, 0.44, and 1.34 ng mL^{-1} were achieved for GFAP, h-FABP and S100 β biomarker, respectively. The evident loss of sensitivity (compared to the MSD platform) could likely be attributed to the less performant μ STAT-ECL photodiode versus MSD CCD detector systems. On the other hand, new, highly sensitive and compact detectors in development will likely soon unfold possibilities for low pg mL^{-1} level LODs in POC diagnostic assays. Alternatively, for SPCEs to be applicable for detection of a mTBI-relevant biomarker panel at the clinically relevant concentration ranges (lower pg mL^{-1} range), further developments with ECL signal amplification strategies (e.g., exploring nanomaterials that have a higher capacity for loading of luminophores—e.g., solid-state luminophores) would be highly beneficial.

In terms of the simultaneous detection of multiple analytes, a variety of analytical technologies have been exploited, including fluorescence [61,62], electrochemistry [63,64], surface plasmon resonance [65], and chemiluminescence [66]. However, some techniques need expensive detectors or light sources, while at the same time may suffer insufficient sensitivity for measuring clinical samples. Electrochemiluminescence has shown an excellent potential thanks to the good selectivity and the fact that signal generation can be adjusted by the alternation of the trigger potential, allowing control over emission location and thus enabling multi-analyte detection from the sample, by employing single or multiple

electrodes [67]. The methodologies for ECL-based multiplex assays can be mainly categorized as spatial-resolved, potential-resolved, spectrum-resolved, and other miscellaneous strategies [67]. Herein the spatially resolved approach on a single SPCE has been applied for the first time for multiplex ECL detection of three mTBI biomarkers. Translation of three individual *singleplex* assays into multiplex assay has been successfully done, indicating that such an approach could be further explored for detection of mTBI biomarker panel from limited sample volume (e.g., capillary blood sample, cerebrospinal fluid, etc.), and with the option to extend the biomarker panel and improve the clinical specificity of the test (e.g., fewer false positives).

Due to the differences in mTBI biomarker release kinetics, a multi-point detection at different time intervals after the injury would be an important requirement. For example, GFAP is present in serum samples at detectable concentrations ($>30 \text{ pg mL}^{-1}$) even within 1 h of injury [68], while for S100 β only 12–36 h after trauma. The methodology could certainly benefit both clinicians and patients by being easily extended to other multi-target panels (cancer, cardiac disease, etc.). The spatially resolved approach evidently brings the requirement for the use of a CCD camera and for POC diagnostic applications, it would be necessary to employ a miniaturized and performant detector device and a cartridge unit that would handle all the sample processing steps.

5. Conclusions

Herein, electrochemiluminescence assays for detection of mTBI biomarkers (GFAP, h-FABP, S100 β) have been developed and optimized on the MesoScale Discovery (MSD) platform in 96-well plate format, and on SPCE electrodes combined with μ STAT-ECL from Metrohm DropSens. A “proof-of-concept” for the development of a multiplex ECL assay on a single electrode has been shown. Obtained data could serve as a steppingstone towards the development of an ECL-based POC diagnostic device for multiplex detection of mTBI biomarkers, which can be employed as a diagnostic screening test, but also aid the preclinical evaluation of currently investigated biomarkers and in the establishment of an ‘ideal’ biomarker panel for TBI diagnostics (or adapted for the detection of other biomarker panels in different clinical body fluids).

Supplementary Materials: The following supporting information are available online at <https://www.mdpi.com/article/10.3390/bios12030172/s1>, Table S1: Summary of GFAP, h-FABP and S100 β sensors developed in the last 10 years and their analytical performances; Figure S1: Four-parameter (4PL) dose-response nonlinear regression model for MSD calibration curves; Figure S2: Electrochemical characterization of commercially available screen-printed electrodes (SPE) for ECL applications; Figure S3: SEM images of commercially available Screen-Printed Carbon Electrodes (SPCEs) for ECL applications; Figure S4: Linear regression model for SPCE μ STAT-ECL calibration curves; Figure S5: Results of the recovery studies; Figure S6: CAD drawing of incubation cells used for SPEs. References [27,30–32,54–58,69–119] are cited in the supplementary materials.

Author Contributions: Conceptualization, M.J., D.P. and M.E.P.; methodology, M.J., E.S. and D.P.; writing—original draft preparation, M.J. and E.S.; writing—review and editing, D.P. and M.E.P.; supervision, M.E.P.; project administration, M.E.P.; funding acquisition, M.E.P. All authors have read and agreed to the published version of the manuscript.

Funding: This research was funded by BRIDGE (joint programme conducted by the Swiss National Science Foundation (SNSF) and Innosuisse—the Swiss Innovation Agency), grant No. 40B2-0_181013.

Institutional Review Board Statement: Not applicable.

Informed Consent Statement: Not applicable.

Data Availability Statement: The experimental data is contained within the article.

Acknowledgments: The authors would like to thank Alexandre Nicollier (HES-SO Valais-Wallis), Joana Soares da Silva (HES-SO Valais-Wallis), Léa Loiseau (HES-SO Valais-Wallis), and Aurélie Cino (Université de Genève) for their technical support with the execution of immunoassay experiments.

The authors would also like to thank the mechanical workshop of HES-SO Valais-Wallis for the fabrication of customized incubation cell for SPEs.

Conflicts of Interest: The authors declare no conflict of interest.

References

1. Traumatic Brain Injury. Fact Sheets and Policy Brief. Available online: <https://www.center-tbi.eu/> (accessed on 24 September 2020).
2. Mondello, S.; Muller, U.; Jeromin, A.; Streeter, J.; Hayes, R.L.; Wang, K.K.W. Blood-Based Diagnostics of Traumatic Brain Injuries. *Expert Rev. Mol. Diagn.* **2011**, *11*, 65–78. [[CrossRef](#)] [[PubMed](#)]
3. Report to Congress: Traumatic Brain Injury in the United States | Concussion | Traumatic Brain Injury | CDC Injury Center. Available online: https://www.cdc.gov/traumaticbraininjury/pubs/tbi_report_to_congress.html (accessed on 15 April 2021).
4. Mehta, R.; Trainee1, G.P.; Chinthapalli, K.; Neurologist2, C. Glasgow Coma Scale Explained. *BMJ* **2019**, *365*, l1296. [[CrossRef](#)] [[PubMed](#)]
5. Dewan, M.C.; Rattani, A.; Gupta, S.; Baticulon, R.E.; Hung, Y.-C.; PUNCHAK, M.; Agrawal, A.; Adeleye, A.O.; Shrime, M.G.; Rubiano, A.M.; et al. Estimating the Global Incidence of Traumatic Brain Injury. *J. Neurosurg.* **2018**, *130*, 1080–1097. [[CrossRef](#)] [[PubMed](#)]
6. Crossen, M.C.; Winkler, E.A.; Yue, J.K.; Okonkwo, D.O.; Valadka, A.B.; Steyerberg, E.W.; Lingsma, H.F.; Manley, G.T. Development of a Prediction Model for Post-Concussive Symptoms Following Mild Traumatic Brain Injury: A TRACK-TBI Pilot Study. *J. Neurotrauma* **2017**, *34*, 2396–2409. [[CrossRef](#)] [[PubMed](#)]
7. Powell, J.M.; Ferraro, J.V.; Dikmen, S.S.; Temkin, N.R.; Bell, K.R. Accuracy of Mild Traumatic Brain Injury Diagnosis. *Arch. Phys. Med. Rehabil.* **2008**, *89*, 1550–1555. [[CrossRef](#)] [[PubMed](#)]
8. Martinez, B.I.; Martinez, B.I.; Stabenfeldt, S.E. Current Trends in Biomarker Discovery and Analysis Tools for Traumatic Brain Injury. *J. Biol. Eng.* **2019**, *16*, 1–12. [[CrossRef](#)] [[PubMed](#)]
9. Yokobori, S.; Hosein, K.; Burks, S.; Sharma, I.; Gajavelli, S.; Bullock, R. Biomarkers for the Clinical Differential Diagnosis in Traumatic Brain Injury—a Systematic Review. *CNS Neurosci. Ther.* **2013**, *19*, 556–565. [[CrossRef](#)]
10. Tomar, G.S.; Singh, G.P.; Lahkar, D.; Sengar, K.; Nigam, R.; Mohan, M.; Anindya, R. New Biomarkers in Brain Trauma. *Clin. Chim. Acta* **2018**, *487*, 325–329. [[CrossRef](#)]
11. Sharma, R.; Rosenberg, A.; Bennett, E.R.; Laskowitz, D.T.; Acheson, S.K. A Blood-Based Biomarker Panel to Risk-Stratify Mild Traumatic Brain Injury. *PLoS ONE* **2017**, *12*, e0173798. [[CrossRef](#)]
12. Blennow, K.; Brody, D.L.; Kochanek, P.M.; Levin, H.; McKee, A.; Ribbers, G.M.; Yaffe, K.; Zetterberg, H. Traumatic Brain Injuries. *Nat. Rev. Dis. Primers* **2016**, *2*, 1–19. [[CrossRef](#)]
13. Krausz, A.D.; Korley, F.K.; Burns, M.A. The Current State of Traumatic Brain Injury Biomarker Measurement Methods. *Biosensors* **2021**, *11*, 319. [[CrossRef](#)] [[PubMed](#)]
14. Undén, L.; Calcagnile, O.; Undén, J.; Reinstrup, P.; Bazarian, J. Validation of the Scandinavian Guidelines for Initial Management of Minimal, Mild and Moderate Traumatic Brain Injury in Adults. *BMC Med.* **2015**, *13*, 292–301. [[CrossRef](#)] [[PubMed](#)]
15. Ohrt-Nissen, S.; Friis-Hansen, L.; Dahl, B.; Stensballe, J.; Romner, B.; Rasmussen, L.S. How Does Extracerebral Trauma Affect the Clinical Value of S100B Measurements? *Emerg. Med. J.* **2011**, *28*, 941–944. [[CrossRef](#)] [[PubMed](#)]
16. Kahouadji, S.; Salamin, P.; Praz, L.; Coiffier, J.; Frochoux, V.; Durif, J.; Pereira, B.; Arlettaz, L.; Oris, C.; Sapin, V.; et al. S100B Blood Level Determination for Early Management of Ski-Related Mild Traumatic Brain Injury: A Pilot Study. *Front. Neurol.* **2020**, *11*, 856. [[CrossRef](#)]
17. Hasselblatt, M.; Mooren, F.C.; von Ahsen, N.; Keyvani, K.; Fromme, A.; Schwarze-Eicker, K.; Senner, V.; Paulus, W. Serum S100beta Increases in Marathon Runners Reflect Extracranial Release Rather than Glial Damage. *Neurology* **2004**, *62*, 1634–1636. [[CrossRef](#)] [[PubMed](#)]
18. Missler, U.; Wiesmann, M.; Wittmann, G.; Magerkurth, O.; Hagenström, H. Measurement of Glial Fibrillary Acidic Protein in Human Blood: Analytical Method and Preliminary Clinical Results. *Clin. Chem.* **1999**, *45*, 138–141. [[CrossRef](#)]
19. Luoto, T.M.; Raj, R.; Posti, J.P.; Gardner, A.J.; Panenka, W.J.; Iverson, G.L. A Systematic Review of the Usefulness of Glial Fibrillary Acidic Protein for Predicting Acute Intracranial Lesions Following Head Trauma. *Front. Neurol.* **2017**, *8*, 652. [[CrossRef](#)]
20. Mondello, S.; Sorinola, A.; Czeiter, E.; Vámos, Z.; Amrein, K.; Synnot, A.; Donoghue, E.; Sandor, J.; Wang, K.K.; Diaz-Arrastia, R. Blood-Based Protein Biomarkers for the Management of Traumatic Brain Injuries in Adults Presenting to Emergency Departments with Mild Brain Injury: A Living Systematic Review and Meta-Analysis. *J. Neurotrauma* **2021**, *38*, 1086–1106. [[CrossRef](#)]
21. Di Pietro, V.; Yakoub, K.M.; Scarpa, U.; Di Pietro, C.; Belli, A. MicroRNA Signature of Traumatic Brain Injury: From the Biomarker Discovery to the Point-of-Care. *Front. Neurol.* **2018**, *9*, 429. [[CrossRef](#)]
22. Furuhashi, M.; Hotamisligil, G.S. Fatty Acid-Binding Proteins: Role in Metabolic Diseases and Potential as Drug Targets. *Nat. Rev. Drug Discov.* **2008**, *7*, 489–503. [[CrossRef](#)]
23. Lagerstedt, L.; Egea-Guerrero, J.J.; Bustamante, A.; Montaner, J.; Rodriguez-Rodriguez, A.; El Rahal, A.; Turck, N.; Quintana, M.; Garcia-Armengol, R.; Prica, C.M.; et al. H-FABP: A New Biomarker to Differentiate between CT-Positive and CT-Negative Patients with Mild Traumatic Brain Injury. *PLoS ONE* **2017**, *12*, e0175572. [[CrossRef](#)] [[PubMed](#)]

24. Bogoslovsky, T.; Gill, J.; Jeromin, A.; Davis, C.; Diaz-Arrastia, R. Fluid Biomarkers of Traumatic Brain Injury and Intended Context of Use. *Diagnostics* **2016**, *6*, 37. [CrossRef] [PubMed]
25. Posti, J.P.; Takala, R.S.K.; Lagerstedt, L.; Dickens, A.M.; Hossain, I.; Mohammadian, M.; Ala-Seppälä, H.; Frantzén, J.; van Gils, M.; Hutchinson, P.J.; et al. Correlation of Blood Biomarkers and Biomarker Panels with Traumatic Findings on Computed Tomography after Traumatic Brain Injury. *J. Neurotrauma* **2019**, *36*, 2178–2189. [CrossRef] [PubMed]
26. Lagerstedt, L.; Egea-Guerrero, J.J.; Bustamante, A.; Rodríguez-Rodríguez, A.; Rahal, A.E.; Quintana-Díaz, M.; García-Armengol, R.; Prica, C.M.; Andereggen, E.; Rinaldi, L.; et al. Combining H-FABP and GFAP Increases the Capacity to Differentiate between CT-Positive and CT-Negative Patients with Mild Traumatic Brain Injury. *PLoS ONE* **2018**, *13*, e0200394. [CrossRef] [PubMed]
27. Bazarian, J.J.; Biberthaler, P.; Welch, R.D.; Lewis, L.M.; Barzo, P.; Bogner-Flatz, V.; Brolinson, P.G.; Büki, A.; Chen, J.Y.; Christenson, R.H.; et al. Serum GFAP and UCH-L1 for Prediction of Absence of Intracranial Injuries on Head CT (ALERT-TBI): A Multicentre Observational Study. *Lancet Neurol.* **2018**, *17*, 782–789. [CrossRef]
28. Abbott Receives FDA 510(k) Clearance for the First Rapid Handheld Blood Test for Concussions. Available online: <https://abbott.mediaroom.com/2021-01-11-Abbott-Receives-FDA-510-k-Clearance-for-the-First-Rapid-Handheld-Blood-Test-for-Concussions> (accessed on 24 March 2021).
29. Nanodiagnosics Nanosensor Technology | Our Solution. Available online: <https://nanodiagnosics.com/our-solution/nanosensor-technology/> (accessed on 29 March 2021).
30. Pankratova, N.; Jović, M.; Pfeifer, M.E. Electrochemical Sensing of Blood Proteins for Mild Traumatic Brain Injury (MTBI) Diagnostics and Prognostics: Towards a Point-of-Care Application. *RSC Adv.* **2021**, *11*, 17301–17319. [CrossRef] [PubMed]
31. Gan, X.; Han, D.; Wang, J.; Liu, P.; Li, X.; Zheng, Q.; Yan, Y. A Highly Sensitive Electrochemiluminescence Immunosensor for H-FABP Determination Based on Self-Enhanced Luminophore Coupled with Ultrathin 2D Nickel Metal-Organic Framework Nanosheets. *Biosens. Bioelectron.* **2021**, *171*, 112735. [CrossRef] [PubMed]
32. Qin, X.; Zhang, X.; Wang, M.; Dong, Y.; Liu, J.; Zhu, Z.; Li, M.; Yang, D.; Shao, Y. Fabrication of Tris(Bipyridine)Ruthenium(II)-Functionalized Metal-Organic Framework Thin Films by Electrochemically Assisted Self-Assembly Technique for Electrochemiluminescent Immunoassay. *Anal. Chem.* **2018**, *90*, 11622–11628. [CrossRef]
33. Fu, Z.; Wei, W.; Li, C.; Wang, Z. Electrochemiluminescent Immunosensing and Its Application in Biological and Pharmaceutical Analysis. *Sci. Sin.-Chim.* **2011**, *41*, 773–784. [CrossRef]
34. Hoffmann, U.; Espeter, F.; Weiss, C.; Ahmad-Nejad, P.; Lang, S.; Brueckmann, M.; Akin, I.; Neumaier, M.; Borggreffe, M.; Behnes, M. Ischemic Biomarker Heart-Type Fatty Acid Binding Protein (HFABP) in Acute Heart Failure—Diagnostic and Prognostic Insights Compared to NT-ProBNP and Troponin I. *BMC Cardiovasc. Disord.* **2015**, *15*, 50. [CrossRef]
35. Abir, J.; Sondes, S.; Rania, E.; Latifa, K.; Mokhles, B.D.; Nedia, B.; Hadj, B.; Manel, M.; Souhir, K.; Hejer, G.; et al. Serum Heart Type Fatty Acid Binding Protein (H-FABP) Levels in Metabolic Syndrome. *Int. J. Pharm. Sci. Res.* **2017**, *8*, 1441–1448.
36. Wiesmann, M.; Missler, U.; Gottmann, D.; Gehring, S. Plasma S-100b Protein Concentration in Healthy Adults Is Age- and Sex-Independent. *Clin. Chem.* **1998**, *44*, 1056–1058. [CrossRef] [PubMed]
37. Adrian, H.; Marten, K.; Salla, N.; Lasse, V. Biomarkers of Traumatic Brain Injury: Temporal Changes in Body Fluids. *eNeuro* **2016**, *3*, 1–13. [CrossRef] [PubMed]
38. Gordillo-Escobar, E.; Egea-Guerrero, J.J.; Rodríguez-Rodríguez, A.; Murillo-Cabezas, F. Usefulness of Biomarkers in the Prognosis of Severe Head Injuries. *Med. Intensiva* **2016**, *40*, 105–112. [CrossRef] [PubMed]
39. Lewis, L.M.; Schloemann, D.T.; Lindburg, M.; Papa, L.; Fucetola, R.P.; Bazarian, J.; Welch, R.D. Utility of Serum Biomarkers in the Diagnosis and Stratification of Mild Traumatic Brain Injury. *Acad. Emerg. Med.* **2017**, *24*, 710–720. [CrossRef] [PubMed]
40. MSD Technology Platform. Available online: <https://www.mesoscale.com/~{}~/media/files/brochures/techbrochure.pdf> (accessed on 24 September 2020).
41. Neves, M.M.P.S.; Bobes-Limenes, P.; Pérez-Junquera, A.; González-García, M.B.; Hernández-Santos, D.; Fanjul-Bolado, P. Miniaturized Analytical Instrumentation for Electrochemiluminescence Assays: A Spectrometer and a Photodiode-Based Device. *Anal. Bioanal. Chem.* **2016**, *408*, 7121–7127. [CrossRef] [PubMed]
42. Smith, S.P.; Shaw, G.S. A Novel Calcium-Sensitive Switch Revealed by the Structure of Human S100B in the Calcium-Bound Form. *Structure* **1998**, *6*, 211–222. [CrossRef]
43. Gonçalves, D.S.; Lenz, G.; Karl, J.; Gonçalves, C.A.; Rodnight, R. Extracellular S100B Protein Modulates ERK in Astrocyte Cultures. *Neuroreport* **2000**, *11*, 807–809. [CrossRef]
44. Green, A.J.; Keir, G.; Thompson, E.J. A Specific and Sensitive ELISA for Measuring S-100b in Cerebrospinal Fluid. *J. Immunol. Methods* **1997**, *205*, 35–41. [CrossRef]
45. Tramontina, F.; Karl, J.; Gottfried, C.; Mendez, A.; Gonçalves, D.; Portela, L.V.; Gonçalves, C.-A. Digitonin-Permeabilization of Astrocytes in Culture Monitored by Trypan Blue Exclusion and Loss of S100B by ELISA. *Brain Res. Protoc.* **2000**, *6*, 86–90. [CrossRef]
46. Tort, A.B.L.; Dietrich, M.O.; Gonçalves, C.A.; Souza, D.O.; Portela, L.V.C. Influence of Anticoagulants on the Measurement of S100B Protein in Blood. *Clin. Biochem.* **2003**, *36*, 629–632. [CrossRef]
47. Valenti, G.; Fiorani, A.; Li, H.; Sojic, N.; Paolucci, F. Essential Role of Electrode Materials in Electrochemiluminescence Applications. *ChemElectroChem* **2016**, *3*, 1990–1997. [CrossRef]
48. Workman, S.; Richter, M.M. The Effects of Nonionic Surfactants on the Tris(2,2'-Bipyridyl)Ruthenium(II)-Tripropylamine Electrochemiluminescence System. *Anal. Chem.* **2000**, *72*, 5556–5561. [CrossRef] [PubMed]

49. Kerr, E.; Alexander, R.; Francis, P.S.; Guijt, R.M.; Barbante, G.J.; Doeven, E.H. A Comparison of Commercially Available Screen-Printed Electrodes for Electrogenenerated Chemiluminescence Applications. *Front. Chem.* **2021**, *8*, 628483. [[CrossRef](#)] [[PubMed](#)]
50. Banks, C.E.; Davies, T.J.; Wildgoose, G.G.; Compton, R.G. Electrocatalysis at Graphite and Carbon Nanotube Modified Electrodes: Edge-Plane Sites and Tube Ends Are the Reactive Sites. *Chem. Commun.* **2005**, 829–841. [[CrossRef](#)] [[PubMed](#)]
51. Fanjul-Bolado, P.; Hernández-Santos, D.; Lamas-Ardisana, P.J.; Martín-Pernía, A.; Costa-García, A. Electrochemical Characterization of Screen-Printed and Conventional Carbon Paste Electrodes. *Electrochim. Acta* **2008**, *53*, 3635–3642. [[CrossRef](#)]
52. Bard, A.J.; Faulkner, L.R. *Electrochemical Methods: Fundamentals and Applications*, 2nd ed.; John Wiley & Sons: New York, NY, USA, 2001.
53. Zu, Y.; Bard, A.J. Electrogenenerated Chemiluminescence. 67. Dependence of Light Emission of the Tris(2,2′)Bipyridylruthenium(II)/Tripropylamine System on Electrode Surface Hydrophobicity. *Anal. Chem.* **2001**, *73*, 3960–3964. [[CrossRef](#)] [[PubMed](#)]
54. Button, E.B.; Cheng, W.H.; Barron, C.; Cheung, H.; Bashir, A.; Cooper, J.; Gill, J.; Stukas, S.; Baron, D.C.; Robert, J.; et al. Development of a Novel, Sensitive Translational Immunoassay to Detect Plasma Glial Fibrillary Acidic Protein (GFAP) after Murine Traumatic Brain Injury. *Alz. Res. Ther.* **2021**, *13*, 58. [[CrossRef](#)]
55. Elecsys®S100. Available online: <https://diagnostics.roche.com/global/en/products/params/elecsys-s100.html> (accessed on 27 August 2021).
56. Natarajan, S.; Joseph, J. A Novel Time-Resolved Fluorescent Lateral Flow Immunoassay for Quantitative Detection of the Trauma Brain Injury Biomarker-Glial Fibrillary Acidic Protein. *Sens. Diagn.* **2022**, *1*, 193–197. [[CrossRef](#)]
57. Savin, M.; Mihailescu, C.-M.; Matei, I.; Stan, D.; Moldovan, C.A.; Ion, M.; Baciuc, I. A Quantum Dot-Based Lateral Flow Immunoassay for the Sensitive Detection of Human Heart Fatty Acid Binding Protein (HFABP) in Human Serum. *Talanta* **2018**, *178*, 910–915. [[CrossRef](#)]
58. Gao, X.; Boryczka, J.; Zheng, P.; Kasani, S.; Yang, F.; Engler-Chiurazzi, E.B.; Simpkins, J.W.; Wigginton, J.G.; Wu, N. A “Hot Spot”-Enhanced Paper Lateral Flow Assay for Ultrasensitive Detection of Traumatic Brain Injury Biomarker S-100β in Blood Plasma. *Biosens. Bioelectron.* **2021**, *177*, 112967. [[CrossRef](#)] [[PubMed](#)]
59. Mincu, N.-B.; Lazar, V.; Stan, D.; Mihailescu, C.M.; Iosub, R.; Mateescu, A.L. Screen-Printed Electrodes (SPE) for In Vitro Diagnostic Purpose. *Diagnostics* **2020**, *10*, 517. [[CrossRef](#)] [[PubMed](#)]
60. Martínez-Periñán, E.; Gutiérrez-Sánchez, C.; García-Mendiola, T.; Lorenzo, E. Electrochemiluminescence Biosensors Using Screen-Printed Electrodes. *Biosensors* **2020**, *10*, 118. [[CrossRef](#)] [[PubMed](#)]
61. Cao, Z.; Li, H.; Lau, C.; Zhang, Y. Cross-Talk-Free Simultaneous Fluoroimmunoassay of Two Biomarkers Based on Dual-Color Quantum Dots. *Anal. Chim. Acta* **2011**, *698*, 44–50. [[CrossRef](#)] [[PubMed](#)]
62. Wang, S.; Zheng, L.; Cai, G.; Liu, N.; Liao, M.; Li, Y.; Zhang, X.; Lin, J. A Microfluidic Biosensor for Online and Sensitive Detection of Salmonella Typhimurium Using Fluorescence Labeling and Smartphone Video Processing. *Biosens. Bioelectron.* **2019**, *140*, 111333. [[CrossRef](#)]
63. Wu, Y.; Xue, P.; Kang, Y.; Hui, K.M. Paper-Based Microfluidic Electrochemical Immunodevice Integrated with Nanobioprobes onto Graphene Film for Ultrasensitive Multiplexed Detection of Cancer Biomarkers. *Anal. Chem.* **2013**, *85*, 8661–8668. [[CrossRef](#)] [[PubMed](#)]
64. Liu, Z.; Rong, Q.; Ma, Z.; Han, H. One-Step Synthesis of Redox-Active Polymer/AU Nanocomposites for Electrochemical Immunoassay of Multiplexed Tumor Markers. *Biosens. Bioelectron.* **2015**, *65*, 307–313. [[CrossRef](#)]
65. Otsuki, S.; Ishikawa, M. Wavelength-Scanning Surface Plasmon Resonance Imaging for Label-Free Multiplexed Protein Microarray Assay. *Biosens. Bioelectron.* **2010**, *26*, 202–206. [[CrossRef](#)]
66. Yang, Z.; Zong, C.; Yan, F.; Ju, H. Automated Chemiluminescent Dual-Analyte Immunoassay Based on Resolved Immunosensing Channels. *Talanta* **2010**, *82*, 1462–1467. [[CrossRef](#)]
67. Lv, W.; Ye, H.; Yuan, Z.; Liu, X.; Chen, X.; Yang, W. Recent Advances in Electrochemiluminescence-Based Simultaneous Detection of Multiple Targets. *TrAC Trends Anal. Chem.* **2020**, *123*, 115767. [[CrossRef](#)]
68. Papa, L.; Brophy, G.M.; Welch, R.D.; Lewis, L.M.; Braga, C.F.; Tan, C.N.; Ameli, N.J.; Lopez, M.A.; Haeussler, C.A.; Giordano, D.I.M. Time Course and Diagnostic Accuracy of Glial and Neuronal Blood Biomarkers GFAP and UCH-L1 in a Large Cohort of Trauma Patients with and without Mild Traumatic Brain Injury. *JAMA Neurol.* **2016**, *73*, 551–560. [[CrossRef](#)] [[PubMed](#)]
69. Arya, S.K.; Pui, T.S.; Wong, C.C.; Kumar, S.; Rahman, A.R.A. Effects of the Electrode Size and Modification Protocol on a Label-Free Electrochemical Biosensor. *Langmuir* **2013**, *29*, 6770–6777. [[CrossRef](#)] [[PubMed](#)]
70. Huang, W.; Besar, K.; LeCover, R.; Dulloor, P.; Sinha, J.; Martínez Hardigree, J.F.; Pick, C.; Swavola, J.; Everett, A.D.; Frechette, J.; et al. Label-Free Brain Injury Biomarker Detection Based on Highly Sensitive Large Area Organic Thin Film Transistor with Hybrid Coupling Layer. *Chem. Sci.* **2014**, *5*, 416–426. [[CrossRef](#)]
71. Wang, T.; Fang, Y.; He, Z. Electrochemical Quantitative Detection of Glial Fibrillary Acidic Protein Based on Molecularly Imprinted Polymer Sensor. *Int. J. Electrochem. Sci.* **2017**, *12*, 7341–7350. [[CrossRef](#)]
72. Song, J.; Dailey, J.; Li, H.; Jang, H.-J.; Zhang, P.; Wang, J.T.-H.; Everett, A.D.; Katz, H.E. Extended Solution Gate OFET-Based Biosensor for Label-Free Glial Fibrillary Acidic Protein Detection with Polyethylene Glycol-Containing Bioreceptor Layer. *Adv. Funct. Mater.* **2017**, *27*, 1606506. [[CrossRef](#)] [[PubMed](#)]

73. Khetani, S.; Ozhukil Kollath, V.; Kundra, V.; Nguyen, M.D.; Debert, C.; Sen, A.; Karan, K.; Sanati-Nezhad, A. Polyethylenimine Modified Graphene-Oxide Electrochemical Immunosensor for the Detection of Glial Fibrillary Acidic Protein in Central Nervous System Injury. *ACS Sens.* **2018**, *3*, 844–851. [CrossRef] [PubMed]
74. Ma, Y.; Xu, G.; Wei, F.; Cen, Y.; Song, Y.; Ma, Y.; Xu, X.; Shi, M.; Sohail, M.; Hu, Q. Carbon Dots Based Immunosorbent Assay for the Determination of GFAP in Human Serum. *Nanotechnology* **2018**, *29*, 145501. [CrossRef]
75. Cardinell, B.A.; Addington, C.P.; Stabenfeldt, S.E.; La Belle, J.T. Multi-Biomarker Detection Following Traumatic Brain Injury. *Crit. Rev. Biomed. Eng.* **2019**, *47*, 193–206. [CrossRef] [PubMed]
76. Agostini, M.; Amato, F.; Vieri, M.L.; Greco, G.; Tonazzini, I.; Baroncelli, L.; Caleo, M.; Vannini, E.; Santi, M.; Signore, G.; et al. Glial-Fibrillary-Acidic-Protein (GFAP) Biomarker Detection in Serum-Matrix: Functionalization Strategies and Detection by an Ultra-High-Frequency Surface-Acoustic-Wave (UHF-SAW) Lab-on-Chip. *Biosens. Bioelectron.* **2021**, *172*, 112774. [CrossRef]
77. Krausz, A.D.; Korley, F.K.; Burns, M.A. A Variable Height Microfluidic Device for Multiplexed Immunoassay Analysis of Traumatic Brain Injury Biomarkers. *Biosensors* **2021**, *11*, 320. [CrossRef] [PubMed]
78. GFAP ELISA Kit | Sigma-Aldrich. Available online: <https://www.sigmaaldrich.com/HK/zh/life-science/supelco> (accessed on 30 August 2021).
79. R-PLEX Human GFAP Antibody Set | Meso Scale Discovery. Available online: <https://www.mesoscale.com/en/products/r-plex-human-gfap-antibody-set-f211m/> (accessed on 31 August 2021).
80. Available online: https://www.Banyanbio.Com/Assets/Files/000175_vA-IFU-Banyan-BTI.Pdf (accessed on 27 April 2020).
81. Simoa Technology. Available online: <https://www.Quanterix.Com/Technology> (accessed on 27 April 2020).
82. TBI Plasma Cartridge | Abbott Point of Care. Available online: <https://www.pointofcare.abbott/us/en/offerings/istat/istat-test-cartridges/TBI-Plasma> (accessed on 30 August 2021).
83. Okonkwo, D.O.; Puffer, R.C.; Puccio, A.M.; Yuh, E.L.; Yue, J.K.; Diaz-Arrastia, R.; Korley, F.K.; Wang, K.K.W.; Sun, X.; Taylor, S.R.; et al. Point-of-Care Platform Blood Biomarker Testing of Glial Fibrillary Acidic Protein versus S100 Calcium-Binding Protein B for Prediction of Traumatic Brain Injuries: A Transforming Research and Clinical Knowledge in Traumatic Brain Injury Study. *J. Neurotrauma* **2020**, *37*, 2460–2467. [CrossRef] [PubMed]
84. Korley, F.K.; Datwyler, S.A.; Jain, S.; Sun, X.; Beligere, G.; Chandran, R.; Marino, J.A.; McQuiston, B.; Zhang, H.; Caudle, K.L.; et al. Comparison of GFAP and UCH-L1 Measurements from Two Prototype Assays: The Abbott i-STAT and ARCHITECT Assays. *Neurotrauma Rep.* **2021**, *2*, 193–199. [CrossRef] [PubMed]
85. Miller, C.J.; Hu, J. Magnetic Immunosensor and Method of Use. U.S. Patent 9,958,440, 2018.
86. The NanoDx™ System for TBI | Our Solution. Available online: <https://nanodiagnosics.com/our-solution/the-nanodx-system-for-tbi/> (accessed on 30 August 2021).
87. Feng, L.-N.; Bian, Z.-P.; Peng, J.; Jiang, F.; Yang, G.-H.; Zhu, Y.-D.; Yang, D.; Jiang, L.-P.; Zhu, J.-J. Ultrasensitive Multianalyte Electrochemical Immunoassay Based on Metal Ion Functionalized Titanium Phosphate Nanospheres. *Anal. Chem.* **2012**, *84*, 7810–7815. [CrossRef] [PubMed]
88. Stan, D.; Mihailescu, C.-M.; Iosub, R.; Moldovan, C.; Savin, M.; Baciu, I. Electrochemical Studies of Homogeneous Self-Assembled Monolayers versus Mixed Self-Assembled Monolayers on Gold Electrode for “Label Free” Detection of Heart Fatty Acid Binding Protein. *Thin Solid Film.* **2012**, *526*, 143–149. [CrossRef]
89. Carless, D.R.; Wnęk, M.; Knox, C.; Harrison, K.R.; Calder, N.; Hall, A.S.; Barth, J.H. Clinical and Analytical Evaluation of an Immunoturbidimetric Heart-Type Fatty Acid-Binding Protein Assay. *Scand. J. Clin. Lab. Investig.* **2013**, *73*, 48–53. [CrossRef] [PubMed]
90. Mihailescu, C.-M.; Stan, D.; Iosub, R.; Moldovan, C.; Savin, M. A Sensitive Capacitive Immunosensor for Direct Detection of Human Heart Fatty Acid-Binding Protein (h-FABP). *Talanta* **2015**, *132*, 37–43. [CrossRef] [PubMed]
91. Qin, X.; Xu, A.; Liu, L.; Sui, Y.; Li, Y.; Tan, Y.; Chen, C.; Xie, Q. Selective Staining of CdS on ZnO Biolabel for Ultrasensitive Sandwich-Type Amperometric Immunoassay of Human Heart-Type Fatty-Acid-Binding Protein and Immunoglobulin G. *Biosens. Bioelectron.* **2017**, *91*, 321–327. [CrossRef] [PubMed]
92. Crapnell, R.D.; Canfarotta, F.; Czulak, J.; Johnson, R.; Betlem, K.; Mecozzi, F.; Down, M.P.; Eersels, K.; van Grinsven, B.; Cleij, T.J.; et al. Thermal Detection of Cardiac Biomarkers Heart-Fatty Acid Binding Protein and ST2 Using a Molecularly Imprinted Nanoparticle-Based Multiplex Sensor Platform. *ACS Sens.* **2019**, *4*, 2838–2845. [CrossRef] [PubMed]
93. Li, F.; Guo, L.; Hu, Y.; Li, Z.; Liu, J.; He, J.; Cui, H. Multiplexed Chemiluminescence Determination of Three Acute Myocardial Infarction Biomarkers Based on Microfluidic Paper-Based Immunodevice Dual Amplified by Multifunctionalized Gold Nanoparticles. *Talanta* **2020**, *207*, 120346. [CrossRef] [PubMed]
94. TBICheck—The Fastest Diagnostic Test for Traumatic Brain Injury. Available online: <https://tbicheck.com/home> (accessed on 30 August 2021).
95. Human H-FABP ELISA Kit (Ab243682) | Abcam. Available online: https://www.abcam.com/Human-H-FABP-ELISA-Kit-ab243682.html?gclid=aw.ds\T1\textbar{}aw.ds&gclid=Cj0KCQJwg7KJBhDyARIsAHrAXaH7SK6R4I_1DbOvLN1pxlnqW42hdrT0Nk4Yjew7t-yxwT-aoeUn4EaAuTJEALw_wcB (accessed on 30 August 2021).
96. R-PLEX Human FABP3/H-FABP Antibody Set | Meso Scale Discovery. Available online: <https://www.mesoscale.com/en/products/r-plex-human-fabp3-h-fabp-antibody-set-f214t/> (accessed on 31 August 2021).
97. Missler, U.; Wiesmann, M.; Friedrich, C.; Kaps, M. S-100 Protein and Neuron-Specific Enolase Concentrations in Blood as Indicators of Infarction Volume and Prognosis in Acute Ischemic Stroke. *Stroke* **1997**, *28*, 1956–1960. [CrossRef] [PubMed]

98. PII: S0022-1759(97)00050-1 | Elsevier Enhanced Reader. Available online: <https://reader.elsevier.com/reader/sd/pii/S0022175997000501?token=A464853B1ED8E1A9E89C9B8F041BB4E0DF5188385648EF4C35723E513BFC3977CFC76D86BA77D9A85AFD7B71FF48711E&originRegion=eu-west-1&originCreation=20210827152016> (accessed on 27 August 2021).
99. Leite, M.C.; Galland, F.; Brolese, G.; Guerra, M.C.; Bortolotto, J.W.; Freitas, R.; de Almeida, L.M.V.; Gottfried, C.; Gonçalves, C.-A. A Simple, Sensitive and Widely Applicable ELISA for S100B: Methodological Features of the Measurement of This Glial Protein. *J. Neurosci. Methods* **2008**, *169*, 93–99. [[CrossRef](#)] [[PubMed](#)]
100. Liu, Y.; Wang, H.; Chen, J.; Liu, C.; Li, W.; Kong, J.; Yang, P.; Liu, B. A Sensitive Microchip-Based Immunosensor for Electrochemical Detection of Low-Level Biomarker S100B. *Electroanalysis* **2013**, *25*, 1050–1055. [[CrossRef](#)]
101. Wang, X.; Li, H.; Li, X.; Chen, Y.; Yin, Y.; Li, G. Electrochemical Assay of Melanoma Biomarker in Human Blood. *Electrochem. Commun.* **2014**, *39*, 12–14. [[CrossRef](#)]
102. Mikula, E.; Wyslouch-Cieszyńska, A.; Zhukova, L.; Puchalska, M.; Verwilt, P.; Dehaen, W.; Radecki, J.; Radecka, H. Voltammetric Detection of S100B Protein Using His-Tagged Receptor Domains for Advanced Glycation End Products (RAGE) Immobilized onto a Gold Electrode Surface. *Sensors* **2014**, *14*, 10650–10663. [[CrossRef](#)] [[PubMed](#)]
103. Kim, C.; Searson, P.C. Magnetic Bead-Quantum Dot Assay for Detection of a Biomarker for Traumatic Brain Injury. *Nanoscale* **2015**, *7*, 17820–17826. [[CrossRef](#)] [[PubMed](#)]
104. Kurzątkowska, K.; Jankowska, A.; Wyslouch-Cieszyńska, A.; Zhukova, L.; Puchalska, M.; Dehaen, W.; Radecka, H.; Radecki, J. Voltammetric Detection of the S100B Protein Using His-Tagged RAGE Domain Immobilized onto a Gold Electrode Modified with a Dipyrromethene—Cu(II) Complex and Different Diluents. *J. Electroanal. Chem.* **2016**, *767*, 76–83. [[CrossRef](#)]
105. Khetani, S.; Aburashed, R.; Singh, A.; Sen, A.; Sanati-Nezhad, A. Immunosensing of S100 β Biomarker for Diagnosis of Spinal Cord Injuries (SCI). *Sens. Actuators B Chem.* **2017**, *247*, 163–169. [[CrossRef](#)]
106. Kuo, Y.-C.; Lee, C.-K.; Lin, C.-T. Improving Sensitivity of a Miniaturized Label-Free Electrochemical Biosensor Using Zigzag Electrodes. *Biosens. Bioelectron.* **2018**, *103*, 130–137. [[CrossRef](#)] [[PubMed](#)]
107. Wang, Y.; Zhao, P.; Mao, L.; Hou, Y.; Li, D. Determination of Brain Injury Biomarkers by Surface-Enhanced Raman Scattering Using Hollow Gold Nanospheres. *RSC Adv.* **2018**, *8*, 3143–3150. [[CrossRef](#)]
108. Mathew, A.S.; Shi, X.; Yau, S.-T. Detection of a Traumatic Brain Injury Biomarker at the 10 Fg/ML Level. *Mol. Diagn. Ther.* **2018**, *22*, 729–735. [[CrossRef](#)]
109. Sun, J.; Zhao, Y.; Hou, Y.; Li, H.; Yang, M.; Wang, Y.; Sun, B. Multiplexed Electrochemical and SERS Dual-Mode Detection of Stroke Biomarkers: Rapid Screening with High Sensitivity. *New J. Chem.* **2019**, *43*, 13381–13387. [[CrossRef](#)]
110. Tabrizi, M.A.; Ferré-Borrull, J.; Kapruwan, P.; Marsal, L.F. A Photoelectrochemical Sandwich Immunoassay for Protein S100 β , a Biomarker for Alzheimer’s Disease, Using an ITO Electrode Modified with a Reduced Graphene Oxide-Gold Conjugate and CdS-Labeled Secondary Antibody. *Microchim. Acta* **2019**, *186*, 117. [[CrossRef](#)] [[PubMed](#)]
111. Harpaz, D.; Koh, B.; Marks, R.S.; Seet, R.C.S.; Abdulhalim, I.; Tok, A.I.Y. Point-of-Care Surface Plasmon Resonance Biosensor for Stroke Biomarkers NT-ProBNP and S100 β Using a Functionalized Gold Chip with Specific Antibody. *Sensors* **2019**, *19*, 2533. [[CrossRef](#)] [[PubMed](#)]
112. Han, L.; Ding, C.; Guo, Y.; Wang, Y.; Ding, Y. Sensitive Detecting MTBI Biomarker S100B by Using Peptide-Modified Ratiometric Fluorescent C/AuNCs Nanoprobe. *Anal Bioanal Chem* **2020**, *412*, 3695–3702. [[CrossRef](#)] [[PubMed](#)]
113. Hassanain, W.A.; Sivanesan, A.; Ayoko, G.A.; Izake, E.L. Rapid Electrochemical Nanosensing of S100 β in Blood. *J. Electrochem. Soc.* **2020**, *167*, 067518. [[CrossRef](#)]
114. Delefortrie, Q.; Lejeune, F.; Kerzmann, B.; Levy, R.; Adam, J.-F.; Sottiaux, T.; Grimmelprez, A.; Vankerhoven, P.; Hachimi-Idrissi, S. Evaluation of the Roche[®] Elecsys and the Diasorin[®] Liaison S100 Kits in the Management of Mild Head Injury in the Emergency Room. *Clin. Biochem.* **2018**, *52*, 123–130. [[CrossRef](#)] [[PubMed](#)]
115. CanAg@S100 EIA | Fujirebio. Available online: <https://www.fujirebio.com/en/products-solutions/canag-s100-eia> (accessed on 27 August 2021).
116. Human S100B ELISA, EZHS100B-33K This Human S100B ELISA Kit Is to Be Used for the Quantification of Human S100B in Cerebrospinal Fluid, Serum & Plasma. | Sigma-Aldrich. Available online: <http://www.sigmaaldrich.com/> (accessed on 30 August 2021).
117. S100B ELISA Kit (Ab234573) | Abcam. Available online: <https://www.abcam.com/s100b-elisa-kit-ab234573.html> (accessed on 30 August 2021).
118. Human S100B ELISA Kit by Bioss, Cat. No. BSKH1066 | Lucerna-Chem AG. Available online: <https://lucerna-chem.ch/shop/3438089/human-s100b-elisa-kit> (accessed on 30 August 2021).
119. S100b ELISA Kit (Rabbit) (GWB-KBBVZ1) | Quantitative Sandwich ELISA. Available online: <https://www.genwaybio.com/s100b-elisa-kit-rabbit-gwb-kbbvz1> (accessed on 30 August 2021).